Zeitschrift: Schweizerische mineralogische und petrographische Mitteilungen = Bulletin suisse de minéralogie et pétrographie

Band: 80 (2000)

Heft: 3

Artikel: Metamorphic evolution of the northern Himachal Himalaya : phase equilibria constraints and thermobarometry

Autor: Wyss, Martin

DOI: https://doi.org/10.5169/seals-60971

SCHWEIZ. MINERAL. PETROGR. MITT. 80, 317–350, 2000

Metamorphic evolution of the northern Himachal Himalaya: phase equilibria constraints and thermobarometry

by *Martin Wyss*[1]

Abstract

In the northern Himachal Himalaya, the Himalayan orogen consists of three tectonic domains, the Tethyan Himalaya, the High Himalayan Crystalline and the Lesser Himalayan Sequence, from NE to SW. Along the transect from the Spiti valley through eastern Lahul to the Parvati valley, the metamorphic evolution of these domains was studied in pelitic rocks of the Precambrian to Lower Cambrian Phe Formation and the Proterozoic Berinag Series. In this area four ductile deformational phases occur, including a first phase D_1 of unknown geometry, the NE-verging D_2 stacking of the Shikar Beh Nappe, SW-verging D_3 folding and SW-directed D_4 extrusion of the Crystalline Nappe between the SW-directed Main Central Thrust at the base and NE-directed normal movement in higher crustal levels. Detailed microtextural analyses allow these deformational phases to be related to four stages of metamorphic crystallization M_1 to M_4. Phase equilibria based on discontinuous reactions allow to place constraints on the metamorphic conditions of each stage. The peak conditions of the main metamorphism M_2 in the High Himalayan Crystalline are estimated by thermobarometry.

Metamorphism M_1 reached sillimanite zone peak conditions for metapelites in the High Himalayan Crystalline with temperatures ranging between 620 and 760 °C. From the Tethyan Himalaya downsection to the underlying High Himalayan Crystalline a gradual succession of chlorite, biotite, garnet and kyanite Barrovian metamorphic mineral zones are observed that formed during M_2 and M_3 respectively, indicating a gradual transition between these two domains. As a consequence, the Tethyan Himalaya and the High Himalayan Crystalline represent metamorphic zones rather than tectonic units in the studied area. M_2 is the main metamorphism in the High Himalayan Crystalline. It is a Barrovian-type metamorphism, reaching kyanite zone peak conditions of $T \approx 700$ °C and $P \approx 850$ MPa.

By contrast, M_3 is the main metamorphism in the Tethyan Himalaya. In the High Himalayan Crystalline M_3 peak conditions were close to M_2 conditions within the kyanite zone. During D_4 thrusting of the Crystalline Nappe over the Lesser Himalayan Sequence along the Main Central Thrust, the M_2/M_3 Barrovian kyanite zone mineral assemblage was overprinted by a retrograde M_4 greenschist facies metamorphism at the base of the High Himalayan Crystalline. In the underlying Lesser Himalayan Sequence D_4 shearing was related to a prograde M_4 greenschist facies metamorphism. Concurrently with greenschist facies M_4 overprint along the Main Central Thrust, the M_2/M_3 kyanite zone mineral assemblage was overprinted by a sillimanite-bearing assemblage in NE-dipping D_4 normal shear zones in higher crustal levels. Barometry indicates that D_4 normal shearing was associated with increasing decompression going upsection in the High Himalayan Crystalline. The overgrowth of the M_2/M_3 mineral assemblage by M_4 during extrusion of the Crystalline Nappe results in an apparent inverted metamorphic zonation, from greenschist facies at the base of the High Himalayan Crystalline grading upsection into kyanite- and then into sillimanite zone conditions. M_2 metamorphic peak conditions decrease downsection from $T \approx 700$ °C and $P \approx 850$ MPa to $T \approx 650$ °C and $P \approx 720$ MPa in the kyanite zone. These data suggest that, in addition to the apparent inverted metamorphic zonation caused by M_4 overprint, M_2 isograds were passively deformed during SW-verging D_3 folding and/or during D_4 Crystalline Nappe extrusion, leading to a real inverted metamorphic zonation.

Keywords: polymetamorphism, inverted metamorphic zonation, thermobarometry, P-T path, nappe extrusion, synconvergent extension, Crystalline Nappe, High Himalayan Crystalline, Himachal Pradesh.

1. Introduction

The Himalayan orogen is the result of continental collision between the Indian and Asian plates that began between the latest Paleocene and early Eocene (PATRIAT and ACHACHE 1984; GARZANTI et al. 1987; GARZANTI et al. 1996). The orogen is traditionally subdivided into five laterally contin-

[1] Institut de Minéralogie et Pétrographie, Université de Lausanne, BFSH 2, CH-1015 Lausanne, Switzerland. Present address: Oesterliwaldweg 4, CH-5400 Baden.

Tab. 1 Stratigraphy and petrography of the Tethyan Himalaya (TH), the High Himalayan Crystalline (HHC) and the Lesser Himalayan Sequence (LHS) in the the Spiti valley-eastern Lahul-Parvati valley area. Note the gradual transition between the Tethyan Himalaya and the High Himalayan Crystalline reflected by continuous stratigraphy and by gradually increasing metamorphic conditions.

Age	Formation	Petrography	
Upper Permian	Kuling	Siltstones, pelites, sandstones, limestones, marls	TH
Upper Permian	Ganmachidam	Conglomerates, sandstones	
Middle to Upper Carboniferous	Po	Siltstones, pelites, sandstones, limestones, marls	
Lower Carboniferous	Lipak	Limestones, dolomites, marls, sandstones, shales, gypsum	
Middle Devonian	Muth	Quartzsandstones	
Middle Ordovician	Thaple	Sandstones, siltstones, shales, dolomites	
	Angular unconf.		
Lower Cambrian	Karsha	**Lower chlorite zone:** Siltstones, greywackes, sandstones, dolomites	
Precambrian to Lower Cambrian	Phe	**Lower chlorite zone:** Siltstones, greywackes, sandstones	
		Upper chlorite zone: Slates	
		Biotite zone: Slates, phyllites	
Lower Ordovician Hanuman Tibba intrusion Granites, gneiss		**Garnet zone:** Phyllites, garnet-bearing two-mica schists and biotite schists	HHC
		Kyanite zone: Garnet-, kyanite- and/or sillimanite-bearing two-mica gneisses and schists	
Precambrian	Mélange zone	Quartzite, calcschists, phyllites	LHS
	Berinag Group	Quartzite, biotite-chlorite schists, phyllites	

uous major tectonometamorphic units (GANSSER, 1964; Fig. 1, inset A). These are from north to south: (1) the Indus-Tsangpo Suture Zone (ITSZ), (2) the Tethyan Himalaya (TH), (3) the High Himalayan Crystalline (HHC), (4) the Lesser Himalayan Sequence (LHS) and (5) the Subhimalaya (SH). The Tethyan Himalaya consists of generally nonmetamorphic to low-grade Precambrian to Eocene sediments that were deposited on the northern margin of the Indian continent. The High Himalayan Crystalline represents the high-grade metamorphic zone of the orogen and was thrust over the Lesser Himalayan Sequence along the Main Central Thrust (MCT). The Lesser Himalayan Sequence is thrust over the Subhimalaya along the Main Boundary Thrust (MBT) and the Subhimalaya is thrust over the alluvial deposits of the Indo-Gangetic plain along the Himalayan Frontal Thrust (HFT). Locally, wedged between the High Himalayan Crystalline and the Lesser Himalayan Sequence, a sixth unit, the Lesser Himalayan Crystalline (LHC), occurs (VANNAY and GRASEMANN, 1998).

According to paleomagnetic data (BESSE et al., 1984), approximately 1000 km of the Indian plate margin has been underthrust below and/or accreted to the Asian continent after closing of the Neotethys ocean at the Indus Suture Zone. This shortening caused intracontinental thrusting and nappe formation associated with a polyphase folding and metamorphism within the leading edge of the subducted Indian plate (e.g. EPARD et al., 1995; WYSS et al., 1999). Nappes mainly developed within the High Himalayan Crystalline and the Tethyan Himalaya (FRANK et al., 1973; BASSOULET et al., 1980; STECK et al. 1993).

One of the most debated features of the Himalayan geology is the inverted metamorphic zonation with metamorphic conditions increasing upsection from the Lesser Himalayan Sequence toward the High Himalayan Crystalline and also within the High Himalayan Crystalline, that has been reported from many sections all along the Himalayan orogen. Already observed by MALLET (1875), it has given rise to numerous models that have been proposed in the last 25 years. Some interpretations suggest a mechanical syn- to post metamorphic deformation of isograde through recumbent folding, thrusting or shearing (e.g. FRANK et al., 1977; THÖNI, 1977; BRUNEL and KIENAST, 1986; SEARLE and REX, 1989; TRELOAR et al., 1991; SWAPP and HOLLISTER, 1991; JAIN and MANICKAVASAGAM, 1993; EPARD et al., 1995; GRUJIC et al., 1996; HUBBARD, 1996 and references therein). Other models invoke heat transfer between the hot hanging wall and the colder footwall (LE FORT, 1975) or more complex interactions between the tectonic evolution and thermal processes such as crustal radiogenic heating, heat advection, shear heating and heat focussing (e.g. HUBBARD, 1989; JAMIESON et al., 1996; DAVIDSON et al., 1997 and references therein) or the coupling of pre-deformational thermal disturbances with varying thermal conductivities between different rock types (GRASEMANN, 1993). In the investigated area, a real inversion of isograds occurs, but also an apparent inverted metamorphic zonation is observed, that is the result of a polyphase metamorphic evolution. Accordingly, given the important geological variations observed along the whole Himalayan orogen, it is not surprising, that a great number of models have been proposed until today and that there is little consensus about them.

Another much debated problem is the transition between the Tethyan Himalaya and the High Himalayan Crystalline in eastern Lahul. In the Zanskar area, the Zanskar Shear Zone (Fig. 1) juxtaposed low-grade metamorphic rocks of the Tethyan Himalaya against high-grade metamorphic rocks of the High Himalayan Crystalline by ductile normal shearing, causing a well-defined boundary between these two domains (SEARLE, 1986; HERREN, 1987; SEARLE et al., 1988; SEARLE and REX, 1989; GAPAIS et al., 1992; SEARLE et al., 1992; DÈZES et al., 1999). Consequently, the Tethyan Himalaya and the High Himalayan Crystalline have been interpreted as tectonic units. In order to link the Zanskar Shear Zone with comparable shear zones observed in Garhwal (PÊCHER and SCAILLET, 1989; PÊCHER, 1991; METCALFE, 1993; VANNAY and GRASEMANN, 1998; Fig. 1), SEARLE (1986) and SEARLE et al. (1988) proposed that this structure continues towards SE across eastern Lahul. This contrasts with observations made by HAYDEN (1904), FRANK et al. (1973), FRANK et al. (1977), FUCHS (1987), VANNAY (1993), STECK et al. (1993), VANNAY and STECK (1995) and WYSS et al. (1999), who reported neither a sedimentary nor a tectonometamorphic discontinuity between the Tethyan Himalaya and the High Himalayan Crystalline in Lahul.

Along the Spiti valley–Lahul-Parvati valley section, the polyphase metamorphic evolution of the Tethyan Himalaya and of the High Himalayan Crystalline can be studied in the pelitic Precambrian to Lower Cambrian Phe Formation rocks that occur all along the section. These metapelites recorded a great number of deformational phases and stages of metamorphic crystallization. The evolution of the Lesser Himalayan Sequence is best documented in this area in calcschists and pelitic schists of the Berinag Group.

On the basis of structural, microtextural and petrographic observations on outcrops and in

thin sections, four stages of metamorphic crystallization can be distinguished, that are related to four important phases of deformation. These phases of deformation result from a detailed investigation on the structural evolution of the Spiti valley–Lahul-Parvati valley transect by WYSS et al. (1999). The metamorphic conditions of the four stages of crystallization can be roughly determined on the basis of mineral assemblages. In the High Himalayan Crystalline, a P-T path and peak P-T conditions of the main metamorphism are determined using phase equilibria constraints based on discontinuous reactions and P-T estimates based on mineral chemistry data. The results are discussed with reference to the tectonometamorphic evolution of the Tethyan Himalaya, the High Himalayan Crystalline and the Lesser Himalayan Sequence and with particular emphasis on the inverted metamorphic zonation in the High Himalayan Crystalline and on the transition between the Tethyan Himalaya and the High Himalayan Crystalline.

2. Geological setting

The studied traverse consists of two sections. Section I climbs up from the Spiti river along the Taktsi valley, over Kun Zam La (La = pass) to Batal in eastern Lahul and then down the Upper Chandra valley, over Sara Umga La and down the Tos valley to the Parvati River. Section II

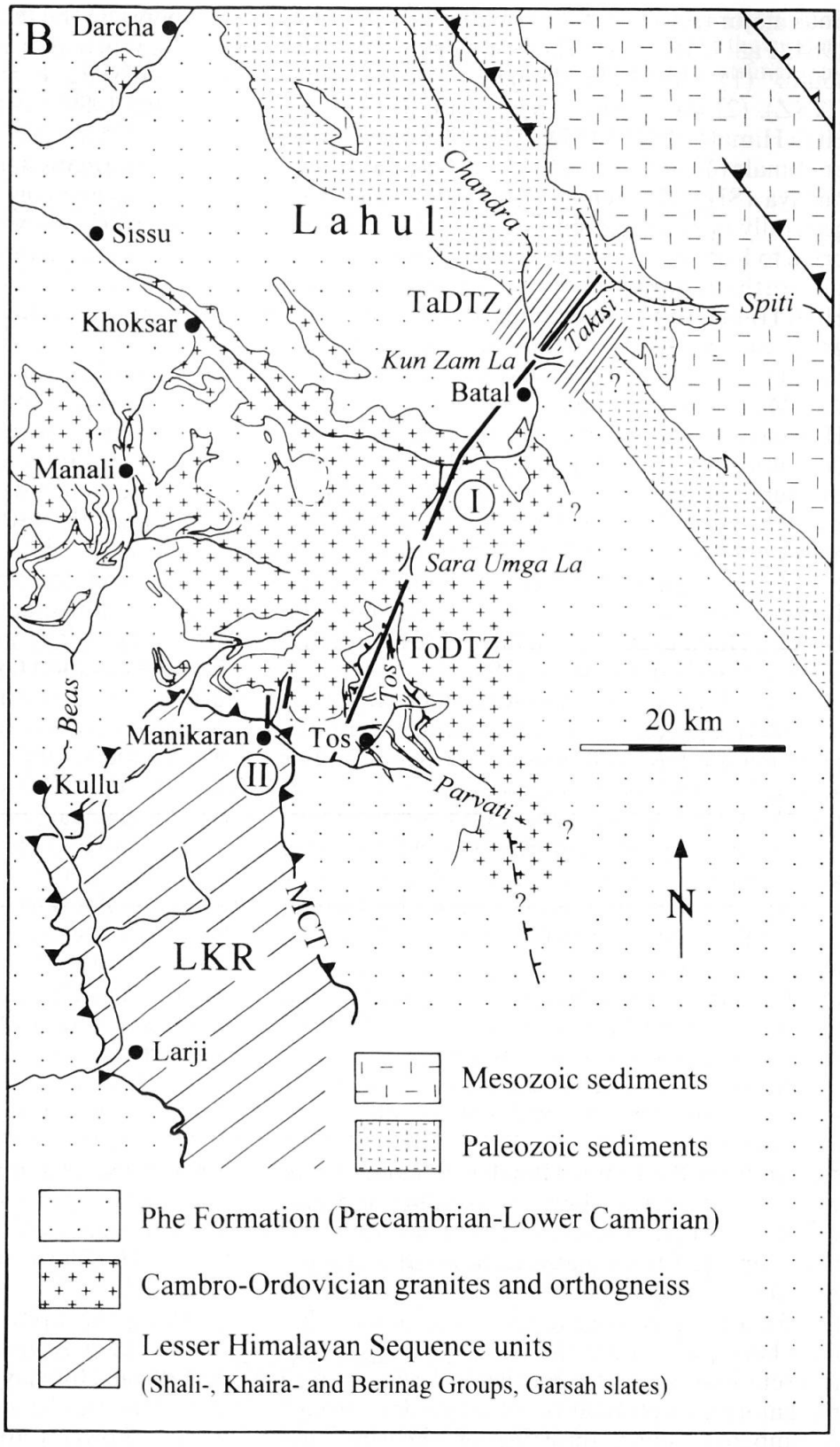

Fig. 1 Generalized map of tectonic zones and mineral zones in the NW Himalaya between Simla and Padum. Mineral zones are compiled after SPRING (1993), STECK et al. (1993), VANNAY (1993), VANNAY and GRASEMANN (1998), DÈZES et al. (1999) and own data. Inset A: Tectonic map of the Himalaya, modified after GUNTLI (1993). Inset B: Geological map of the study area with tracks of the sections I and II indicated (see plate 1). Section II is composite. Compiled after THÖNI (1977), FRANK et al. (1995), VANNAY and STECK (1995) and own data.

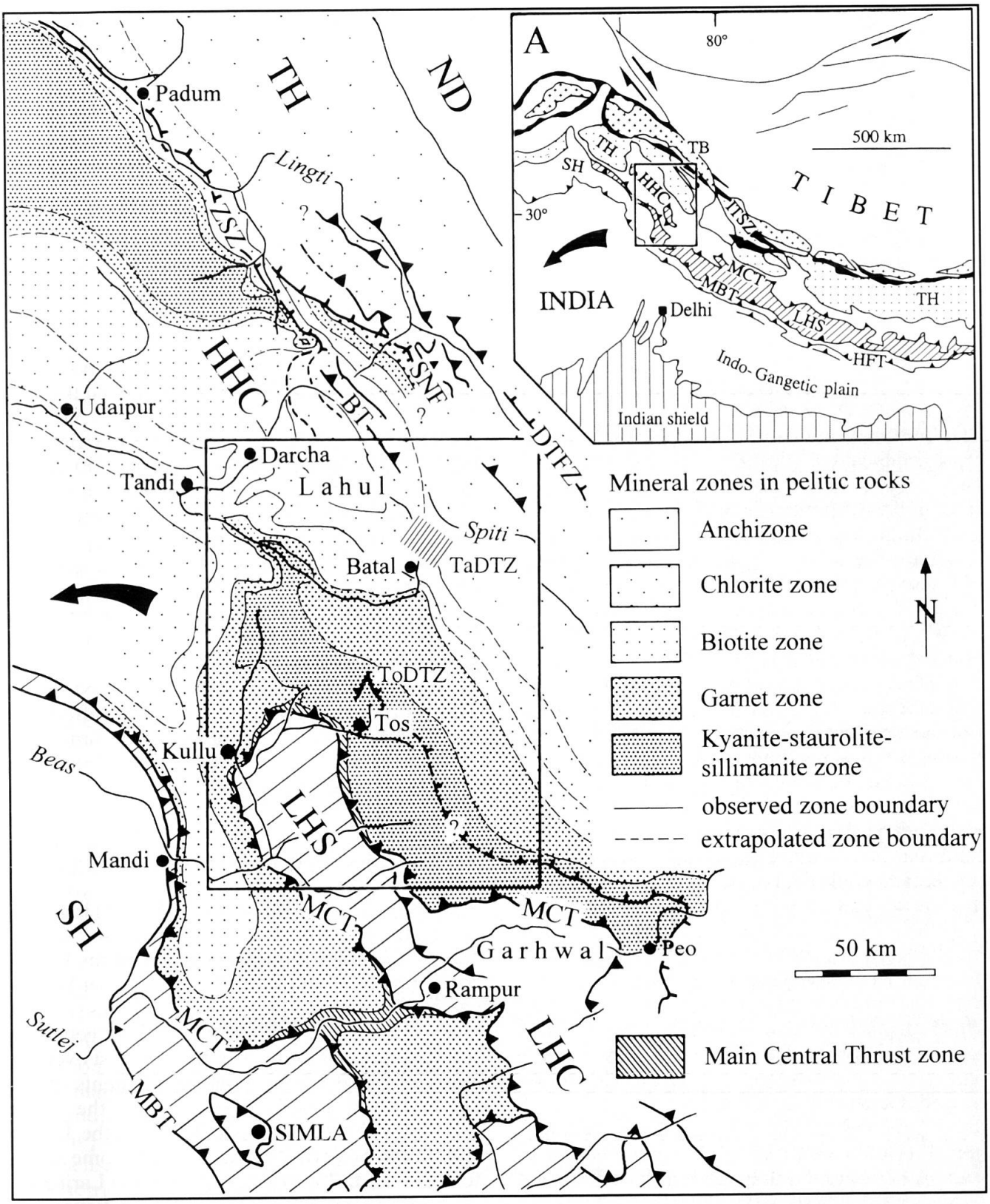

Fig.1 (cont). ND = Nyimaling Dome, TB = Transhimalayan Batholith, TH = Tethyan Himalaya, HHC = High Himalayan Crystalline, LHC = Lesser Himalayan Crystalline, LHS = Lesser Himalayan Sequence, SH = Subhimalaya, LKR = Larji-Kullu-Rampur tectonic window, DTFZ = Dutung-Thaktote Fault Zone, SNF = Sarchu Normal Fault, ZSZ = Zanskar Shear Zone, TaDTZ = Taktsi Dextral Transtension Zone, ToDTZ = Tos Dextral Transtension Zone, BT = Baralacha La Thrust, MCT = Main Central Thrust, MBT = Main Boundary Thrust, HFT = Himalayan Frontal Thrust. Note that the boundary between the Tethyan Himalaya and the High Himalayan Crystalline is well defined along the Zanskar Shear Zone (ZSZ), where it is clearly tectonic. Toward SE, the Zanskar Shear Zone dies out and the transition between these two domains is gradual as indicated by metamorphic mineral zones in metapelitic rocks.

consists of two short sections following the Brahamganga valley N of Manikaran (Fig 1, inset B; Plate 1). Along this traverse, the Tethyan Himalaya, the High Himalayan Crystalline and the Lesser Himalayan Sequence are exposed from the NE to the SW (Fig. 1, Tab. 1). The entire traverse has first been studied in detail by WYSS et al. (1999). Earlier investigations were restricted to the northeasternmost (HAYDEN, 1904; STECK et al., 1993) and southwesternmost areas (FRANK et al., 1973, 1977; THÖNI, 1977).

2.1. LITHOTECTONIC UNITS AND STRATIGRAPHY

2.1.1. Tethyan Himalaya

The Tethyan Himalaya (Fig. 1) is the tectonostratigraphically highest domain of the Himalayan orogen. In the NW Himalaya it represents a stack of north Himalayan nappes that were thrust from the northern edge of the subducted Indian continent towards SW (e.g. the Zanskar Nappes of BASSOULET et al. (1980), the Nyimaling-Tsarap Nappe of STECK et al. (1993) and the Mata Nappe of STECK et al. (1998)). Generally, the Tethyan Himalaya is composed of a nearly complete stratigraphic section of nonmetamorphic or low-grade metamorphic Upper Precambrian to Lower Eocene sediments that were deposited on the northern margin of the Indian plate (GAETANI and GARZANTI, 1991). In the studied area, the Tethyan Himalaya crops out in the Taktsi valley, where it consists of low-grade metamorphic Precambrian to Upper Permian sediments (Tab. 1), the metamorphic degree of which increases from the NE to the SW.

2.1.2. High Himalayan Crystalline

The Tethyan Himalaya is underlain by the High Himalayan Crystalline (Fig. 1), that represents the high-grade metamorphic zone of the Himalayan orogen. Generally, the High Himalayan Crystalline consists of middle- to high-grade metamorphic Precambrian to Jurassic sediments and of Cambro–Ordovician and Tertiary plutonic complexes. (FRANK et al., 1973; STECK et al., 1993). In the studied area, the High Himalayan Crystalline crops out in eastern Lahul, in the Tos valley, in the Parvati valley and in the Brahamganga valley, where it is mainly made up of schists and paragneisses with a metamorphic grade increasing gradually from NE to SW, from greenschist facies to amphibolite facies. These rocks are metamorphic equivalents of the pelitic Precambrian to Lower Cambrian Phe Formation sediments in the Tethyan Himalaya, indicating that the High Himalayan Crystalline represents the stratigraphic continuation of the Tethyan Himalaya downsection (STECK et al., 1993; VANNAY, 1993; WYSS et al., 1999). The rock types in the Phe Formation are summarized in table 1. According to HAYDEN (1904), FRANK et al. (1973, 1977), FUCHS (1987), VANNAY (1993), STECK et al. (1993), VANNAY and STECK (1995) and WYSS et al. (1999), neither a tectonic nor a metamorphic discontinuity occurs between the Tethyan Himalaya and the High Himalayan Crystalline in Lahul and Spiti. The Tethyan Himalaya is therefore considered to be transitional into the underlying High Himalayan Crystalline. Between the Chandra valley in Lahul and the Parvati valley area, the Phe Formation was intruded by the Hanuman Tibba Intrusion of Ordovician age (495 ± 16 Ma, Rb/Sr whole rock isochron, FRANK et al., 1977), which has a well-developed metamorphic contact aureole. WYSS et al. (1999) and WYSS and HERMANN (subm.) reported small mafic intrusions in the lowermost Phe Formation paragneisses of the Tos valley. In the SW, the High Himalayan Crystalline was thrust over the Lesser Himalayan Sequence along the Main Central Thrust with a hanging wall-to-the SW sense of shear, forming the Crystalline Nappe (FRANK, 1973; THÖNI, 1977). Thrusting along the Main Central Thrust affected a zone 4–5 km wide including the High Himalayan Crystalline and the underlying Lesser Himalayan Sequence (WYSS et al, 1999).

2.1.3. Lesser Himalayan Sequence

The Lesser Himalayan Sequence (Fig. 1) is generally made up of the Proterozoic to Lower Cenozoic Gondwanian sedimentary cover of the Indian continent (FRANK et al., 1977, 1995) and of Proterozoic metavolcanics, diabases and granites (FRANK et al., 1977; BHAT and LE FORT, 1992) of generally low metamorphic grade. This unit is thrust over the Paleogene to Neogene molassic sediments of the Subhimalayan foreland basin along the Main Boundary Thrust. In the studied area, the Lesser Himalayan Sequence is exposed in a dome structure that forms the northern part of the Larji-Kullu-Rampur tectonic window (LKR in figure 1), cropping out in the Parvati valley. In this area, it consists of greenschist facies, massive Precambrian quartzites of the Berinag Group, intercalated with pelitic and calc-pelitic schists and phyllites (Tab. 1) that underwent a polyphase structural evolution. On top of the Berinag Quartzites and below the base of the High Himalayan Crystalline a tectonic mélange zone occurs that is made up of lenses of

quartzite surrounded by calcschists and phyllites (WYSS et al., 1999).

2.2. TECTONICS

The studied transect reveals a complex tectonic evolution including an early Himalayan phase D_1, a NE-verging nappe formation D_2, SW-verging folding D_3, SW-directed nappe extrusion D_4 and several late-stage phases. In this chapter an outline of the structural evolution is given based on detailed data presented by WYSS et al. (1999). Fig. 2 is a tectonic model for the phases D_2, D_3 and D_4 based on STECK et al., 1998 and WYSS et al., 1999.

Abbreviations: S = schistosity, cleavage, F = fold, L = lineation, D = deformational phase, M = stage of metamorphic crystallization. Structural elements and stages of metamorphic crystallization that are related to the same deformational phase bear the same number, e.g. S_2, F_2, L_2 and M_2 are related to D_2.

2.2.1. Phase D_1: Early event

The oldest deformation observed in the studied area is documented by a relict schistosity S_1 and by rare isoclinal F_1 folds in the High Himalayan Crystalline. The deformational conditions of D_1 are poorly constrained. However, D_1 is considered to be an important event, since D_1 structures are well recognizable and their imprint is locally very strong although they were overprinted by several subsequent deformational phases.

2.2.2. Phase D_2: NE-verging Shikar Beh Nappe

In the High Himalayan Crystalline, the main deformation is the isoclinal folding F_2 that is related to the main schistosity S_2, to a penetrative, SW–NE-trending (or locally WSW–ENE and W–E-trending) mineral stretching lineation L_2, and to shear sense indicators such as rotated garnets and asymmetrically boudinaged dikes, indicating NE-directed deformation. These structures are interpreted to have formed during NE-directed stacking of the D_2 Shikar Beh Nappe that has first been described by STECK et al. (1993) and VANNAY (1993). It is suggested that NE-directed stacking of the Shikar Beh Nappe occurred contemporaneously with SW-directed stacking of the north Himalayan nappes within the Tethyan Himalaya (STECK et al., 1993, 1998; EPARD et al., 1995). In the Tethyan Himalaya, the existence of D_2 structures is not unambiguously documented.

2.2.3. Phase D_3: Initial stage of Crystalline Nappe formation

The subsequent SW-verging folding F_3 represents a transitional phase of southwestwards propagating deformation between late thrusting at the front of the north Himalayan nappe stack (the Nyimaling-Tsarap Nappe of STECK et al. (1993) and the Mata Nappe of STECK et al. (1998)) and incipient D_4 SW-directed thrusting of the Crystalline Nappe. F_3 folding did not create a nappe structure but large-scale folds that are referred to as the Main Fold Zone. D_3 occurs in both the Tethyan Himalaya and in the High Himalayan Crystalline, documenting the common evolution of these domains during D_3. In the Tethyan Himalaya F_3 folds and the related main schistosity S_3 represent the main phase of deformation. In the High Himalayan Crystalline by contrast, D_3 is of subordinate importance with respect to D_2 and a related schistosity S_3 is rarely observed.

2.2.4. Phase D_4: SW-verging Crystalline Nappe extrusion

During D_4 the Crystalline Nappe was thrust towards SW over the Lesser Himalayan Sequence along the Main Central Thrust. Thrusting on the Main Central Thrust occurred in a zone 4–5 km wide and included both the High Himalayan Crystalline and the underlying Lesser Himalayan Sequence (Fig. 3, Plate 1). It is characterized by a NE–SW-trending mineral stretching lineation and by S-C fabrics, indicating a hanging wall-to-the SW sense of shear. In the Crystalline Nappe stretching lineations and shear bands are concentrated into shear zones some meters to some hundred meters in width, the density of which increases with decreasing distance from the base of the nappe. In the Lesser Himalayan Sequence D_4 shearing is strongest in the schists and phyllites of the mélange zone directly below the base of the Crystalline Nappe. In the underlying Berinag Group, D_4 shear zones are restricted to thin layers of schists and phyllites within the massive Berinag Quartzite (WYSS et al., 1999).

According to WYSS et al. (1999), SW-directed thrusting at the base of the Crystalline Nappe occurred simultaneously with NE-directed dextral transtension in higher crustal levels of the High Himalayan Crystalline and at the transition between the High Himalayan Crystalline and the Tethyan Himalaya. In the High Himalayan Crys-

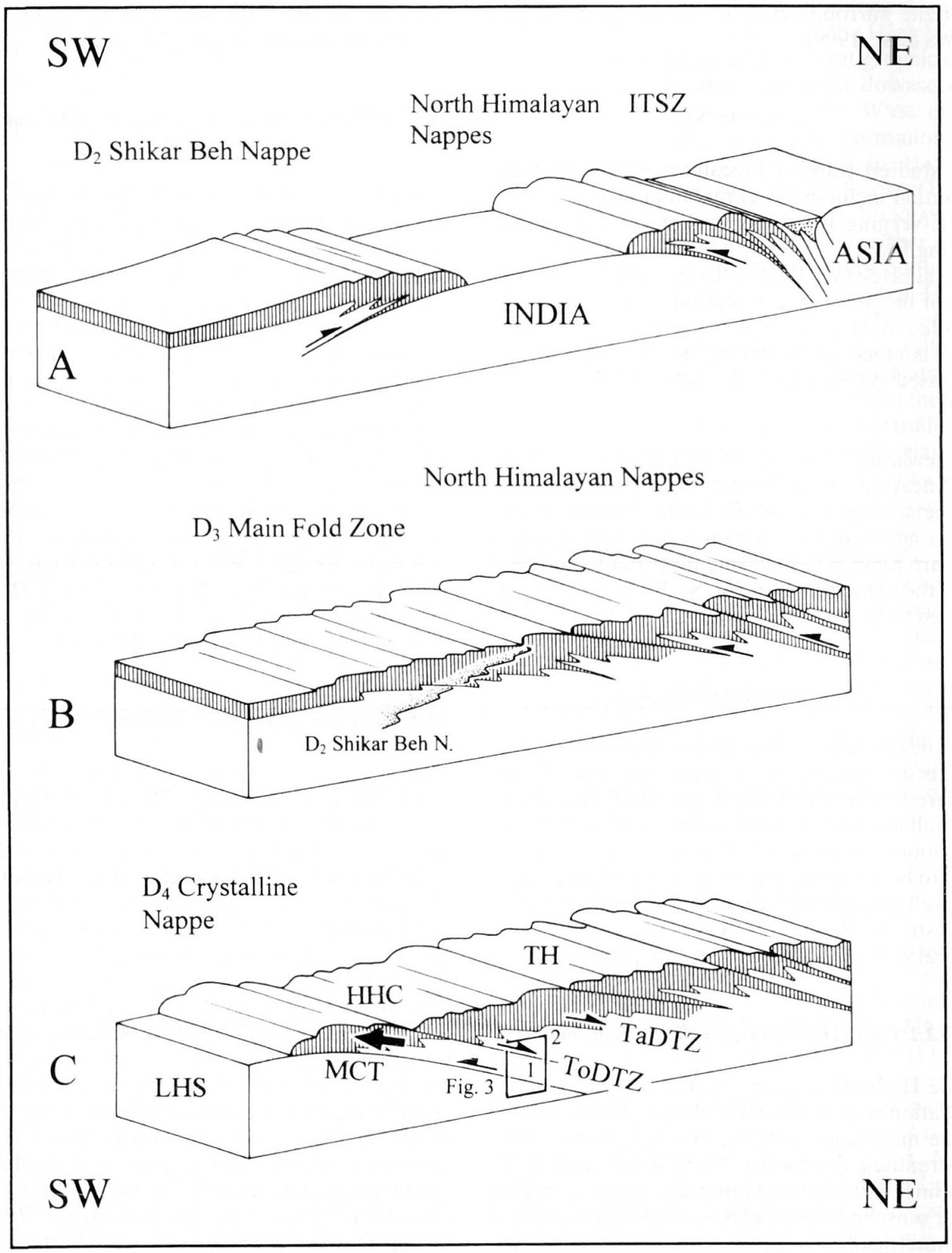

Fig. 2 Model for the tectonic evolution of the NW Himalaya from the Indus Suture Zone (ITSZ) in the NW to the Parvati valley in the SW. Stages B and C focus on the section from the Spiti valley through Lahul to the Parvati valley. The hatched layer is drawn to clarify the geometry of deformation, it has no stratigraphic or tectonic meaning.
(A) Initiation of the NE-verging D_2 Shikar Beh Nappe within the Indian crust SW of the subduction zone and contemporaneous initiation of the SW-verging north Himalayan nappes from the northeastern edge of the Indian crust. The Indian continent was subducted at the base of the north Himalayan nappes. (STECK et al., 1993, 1998; EPARD et al., 1995; WYSS et al., 1999).
(B) Ongoing subduction of the Indian continent at the base of the north Himalayan nappes. The front of the north Himalayan nappes reached the area NE of the front of the Shikar Beh Nappe. Initiation of the D_3 SW-verging Main

talline ductile D_4 dextral transtension is revealed by a ENE-plunging L_4 mineral stretching lineation on NE-dipping shear bands that crosscut S_2, with shear sense criteria indicating a hanging wall down-to-the ENE shear sense. These shear bands are rarely longer than some decimeters, but they are often concentrated locally and combined into huge shear zones of some hundred meters in length and several meters in width. Locally, D_4 dextral shearing rotated L_2 stretching lineations from an originally SW–NE-trending orientation to a W–E-trending orientation. This ductile dextral transtension can be well observed in the Tos valley, where it is distributed over a zone about 5 km wide, referred to as the Tos Dextral Transtension Zone (Fig. 3, Plate 1).

At the transition between the Tethyan Himalaya and the High Himalayan Crystalline, D_4 is characterized by clockwise rotation and NE-directed overturning of formerly SW-verging F_3 folds that occurred in a zone about 6 km wide referred to as the Taktsi Dextral Transtension Zone. The lateral limits of the Taktsi Dextral Transtension Zone are not known, therefore, it is indicated as a diffuse zone in figure 1. Concurrent SW-directed thrusting at the base of the Crystalline Nappe and NE-directed extension in two higher tectonic levels indicate that the Crystalline Nappe was extruded in two parts towards SW between the Lesser Himalayan Sequence and the Tethyan Himalaya (1 and 2 in figure 2,πlate 1).

D_4 transtension is interpreted to be part of a large-scale system of normal and/or dextral strike-slip shear zones that were reported from many sectors of the Himalayan orogen between the Tethyan Himalaya and the High Himalayan Crystalline (e.g. BURG et al., 1984; BRUN et al., 1985; BURCHFIEL and ROYDEN, 1985; SEARLE, 1986; HERREN, 1987; SEARLE et al., 1988; PÊCHER and SCAILLET, 1989; PÊCHER, 1991; PÊCHER et al., 1991; GAPAIS et al., 1992; BURCHFIEL, 1992; METCALFE, 1993), termed the North Himalayan Shear Zone (PÊCHER et al., 1991) or the South Tibetan Detachment System (BURCHFIEL et al., 1992). In these shear zones, normal and/or dextral strike-slip shearing are generally related to a well defined structural detachment that juxtaposes the nonmetamorphic or low-grade metamorphic rocks of the Tethyan Himalaya against high-grade metamorphic rocks of the High Himalayan Crystalline (e.g. the Zanskar Shear Zone: Fig. 1; SEARLE, 1986; HERREN, 1987; SEARLE et al., 1988; SEARLE and REX, 1989; GAPAIS et al., 1992; SEARLE et al., 1992; DÈZES et al., 1999). The Taktsi Dextral Transtension Zone fits well into the Central Himalayan Shear Zone system according to its sense of movement and its tectonic position. However, fold reorientation did not cause a disruption of previous structures. Consequently, in the study area, a tectonic boundary between the Tethyan Himalaya and the High Himalayan Crystalline is not observed.

2.2.5. Late stage phases

D_4 is postdated by a NE-verging backfolding and doming phase, by restarting of SW-directed nappe extrusion and finally by compression parallel to the mountain chain. As none of these phases are related to important stages of metamorphic crystallization, they are not considered here when discussing the metamorphic evolution.

3. Metamorphic petrography

This study focuses on pelitic rocks as they constitute the major part of the rocks exposed along the Spiti valley–Lahul-Parvati valley transect and as they recorded a great number of metamorphic mineral assemblages and deformational structures. The pelitic rocks of the Karsha and Phe Formations make up most of the Tethyan Himalaya in the studied area and the High Himalayan Crystalline is dominated by Phe Formation metapelites. In the Lesser Himalayan Sequence, pelitic schists and phyllites are intercalated with the Berinag Quartzites (Tab. 1). The Karsha Formation consists of metasandstones, metagreywackes and metasiltstones intercalated with dolomite beds. The Phe Formation consists of monotonous alternations of subarkosic to arkosic metasandstones, metagreywackes and metasiltstones with

Fig.2 (cont.)
Fold Zone SW of the north Himalayan nappe stack. D_3 is a southwestward progressing transitional phase between late thrusting of the north Himalayan nappes and early formation of the Crystalline Nappe (WYSS et al., 1999).
(C) Formation of the Main Central Thrust (MCT) and SW-directed D_4 extrusion of the Crystalline Nappe between the Lesser Himalayan Sequence (LHS) and the north Himalayan nappe stack. This is the result of contemporaneous SW-directed thrusting along the Main Central Thrust and NE-directed normal movement in the Tos Dextral Transtension Zone (ToDTZ) and in the Taktsi Dextral Transtension Zone (TaDTZ). As a consequence, the Crystalline Nappe is subdivided into a lower (1) and an upper (2) part (WYSS et al., 1999). During D_4, the zone of subduction has stepped from the base of the north Himalayan nappes to the Main Central Thrust. The TaDTZ has no well defined limits. HHC = High Himalayan Crystalline, corresponding more or less with the Crystalline Nappe; TH = Tethyan Himalaya.

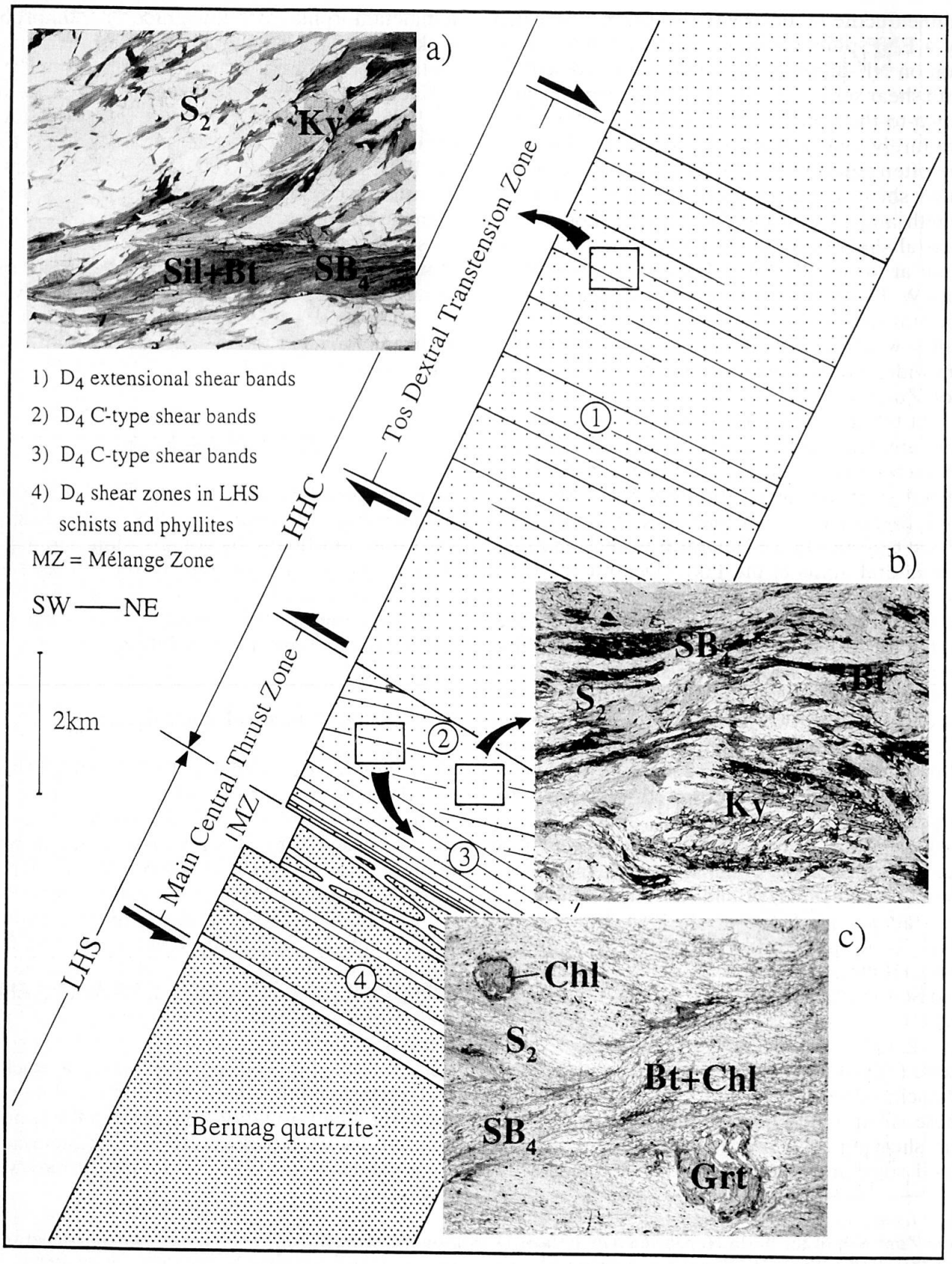

Fig. 3 Simplified section across the Main Central Thrust Zone and the Tos Dextral Transtension Zone (LHS = Lesser Himalayan Sequence, HHC = High Himalayan Crystalline, corresponding to the Crystalline Nappe in the Tos valley–Parvati valley area). Insets: Selected photomicrographs illustrating D_4/M_4. The scale given within brackets corresponds to the long dimension of the images, SW is to the left hand side. (a) Sillimanite and biotite on a D_4 extensional shear band, crosscutting kyanite on S_2 [20 mm]. (b) Kyanite on S_2, partly transformed to muscovite [9.5 mm]. (c) D_4 C'-type shear bands SB_4 crosscutting S_2. Garnet rims are transformed to chlorite [15 mm].

millimeter- to meter-scale bedding that are mostly low-Al pelites (SPEAR, 1993; Fig. 4). Locally, carbonaceous graphitic quartzites and thin marly layers are intercalated. The schists and phyllites intercalated with massive quartzites of the Berinag Group in the Lesser Himalayan Sequence are also low-Al pelites (Fig. 4).

The four tectonic events D_1 to D_4 are documented by structures as well as by the related stages of metamorphic crystallization M_1 to M_4. With the exception of stage M_{1a}, all stages of metamorphic crystallization are related to the formation of a schistosity and are therefore considered to represent syn-tectonic crystallization. Metamorphic main mineral assemblages in the metapelites of the Tethyan Himalaya and the High Himalayan Crystalline allow four prograde Barrovian metamorphic mineral zones to be distinguished. These are, from NE to SW, the chlorite zone, corresponding roughly with the Tethyan Himalaya and the biotite-, garnet- and kyanite zones, corresponding with the High Himalayan Crystalline (Plate 1). In the garnet and kyanite zones, M_2 is the main metamorphism (related to the main schistosity S_2) and consequently, these zones are defined on the basis of the M_2 mineral assemblages. In the chlorite and biotite zones, M_3 is the main metamorphism (related to the main schistosity S_3) and therefore, these zones are defined on the basis of the M_3 mineral assemblages. In the Main Central Thrust Zone, the M_2 kyanite zone assemblage was retrogressively overprinted by a greenschist facies metamorphism at the base of the High Himalayan Crystalline. In the uppermost Lesser Himalayan Sequence, a coeval prograde greenschist facies metamorphism occurred that reached biotite zone conditions (Plate 1).

The interpretation of the pressure and temperature stability conditions of the characteristic assemblages in the metapelites is based on a composite petrogenetic grid adapted to the observed compositions (Fig. 5). Most of the reaction curves limiting these stability fields have a steep dP/dT slope, implying a strong temperature control on the characteristic mineral equilibria.

Mineral abbreviations: Ab = albite, As = aluminosilicate, An = anorthite, Bt = biotite, Carb = carbonate, Chl = chlorite, Cld = chloritoid, Grt = garnet, Kfs = K-feldspar, Ky = kyanite, Ms = muscovite, Pa = paragonite, Phl = phlogopite, Pl = plagioclase, Qtz = quartz, Sil = sillimanite, St = staurolite, Zo = zoisite.

3.1. TETHYAN HIMALAYA AND HIGH HIMALAYAN CRYSTALLINE

3.1.1. Chlorite zone

Lower chlorite zone

In the lower chlorite zone the pelites of the

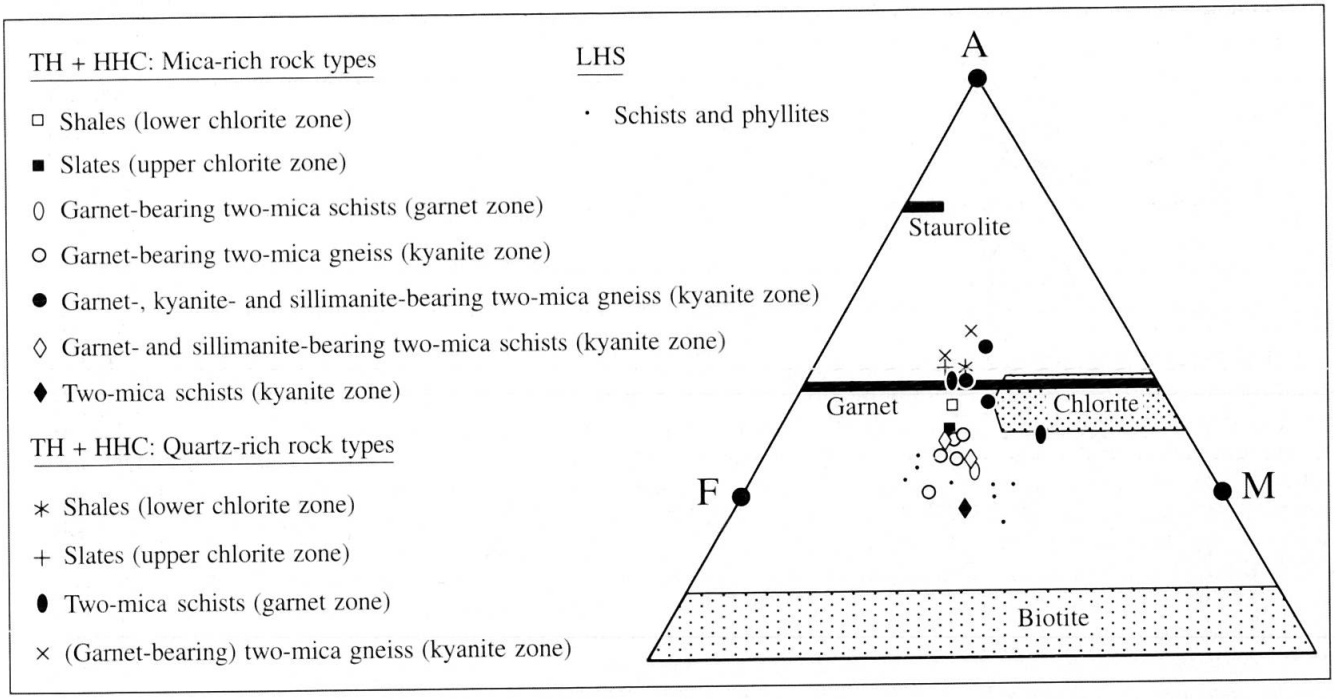

Fig. 4 Bulk compositions of Phe Formation pelites from the Tethyan Himalaya (TH) and the High Himalayan Crystalline (HHC) and of pelitic schists and phyllites from the Berinag Group in the Lesser Himalayan Sequence (LHS), summarized in an AFM diagram. All analyzed samples are low-Al pelites (SPEAR, 1993). The analytical procedure is given in the appendix.

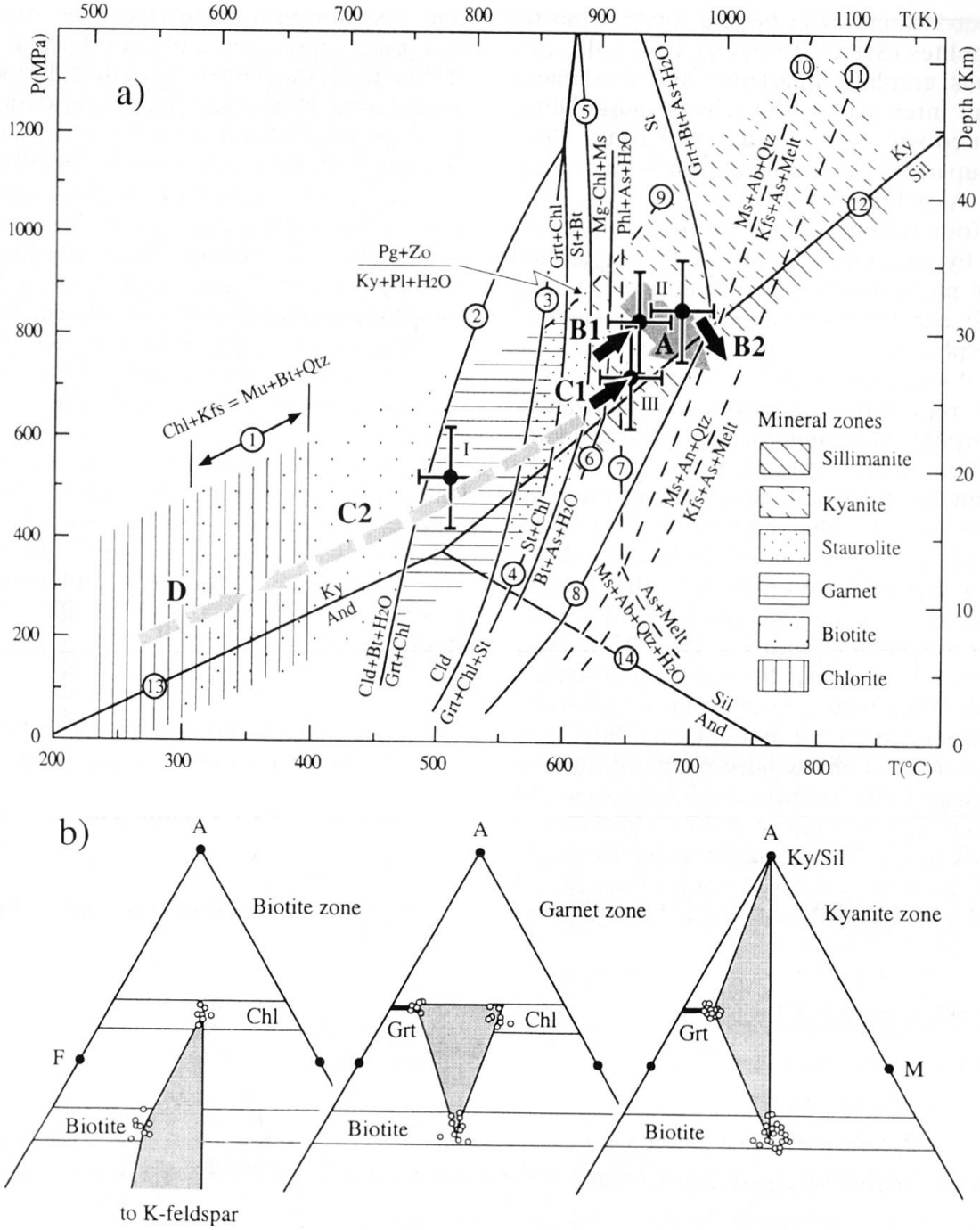

Fig. 5 (a) Composite petrogenetic grid for the metapelites in the Spiti valley-eastern Lahul-Parvati valley area. P-T stability fields for the mineral assemblages characteristic of the observed Barrovian mineral zones are indicated. Solid lines correspond to reactions in the (Mn)KFMASH system and dashed lines correspond to reactions in the CKNASH system. Reactions (2) and (4) that limit the garnet zone field are plotted for $X_{sps} = 0.2$, corresponding to the maximum X_{sps} in the analyzed garnets. Reactions (1) to (6), (8), (9) and (12) to (14) are according to SPEAR and CHENEY (1989) and SPEAR (1993). The vapor present melting reaction (7) represents the minimum conditions for anatexis in water-saturated Ms + Pl + Qtz metapelites and the reactions (10) and (11) correspond to vapor-absent melting conditions (THOMPSON and TRACY, 1979; LE BRETON and THOMPSON, 1988).
P-T estimate I corresponds to sample EMP 1 from the garnet zone, II corresponds to EMP 2 (right) and EMP 8 (left) from the kyanite zone and III corresponds to EMP 11 from the Main Central Thrust Zone. The arrows A–D indicate P-T path segments for the stages of metamorphic crystallization M_1 to M_4 deduced from textural relations discussed in the text. Arrow A: M_{1a}–M_{1b}; arrows B1 and B2: M_2–M_4 in the garnet and kyanite zones and in the Tos Dextral Transtension Zone; arrows C1 and C2: M_2–M_4 in the High Himalayan Crystalline part of the Main Central Thrust Zone; arrow D: M_4 in the Lesser Himalayan Sequence part of the Main Central Thrust Zone. Black arrows are constrained by phase equilibria and P-T estimates, whereas grey arrows indicate qualitative tendencies of P-T paths. (b) Mineral compositions and assemblages characteristic of the biotite-, garnet- and kyanite zones are represented in AFM diagrams. Note the decreasing FeO/(FeO + MgO) ratio in biotite with increasing metamorphic grade.

Phe and Karsha formations display all the characteristics of sedimentary rocks. Graded bedding, rhythmites of alternating sandstones and siltstones as well as cross stratifications are often observed, and on bed surfaces, ripple marks, desiccation cracks, synaersis cracks and trace fossils are abundant. The metasiltstones are slates that display strong cleavages S_2 and S_3 (Fig. 6a), whereas cleavages in more arenitic layers are weak. The rocks mainly consist of detrital monocrystalline grains of quartz, plagioclase, sericitised K-feldspar, muscovite and accessory minerals (detrital rutile, titanite, tourmaline, zircon, apatite, epidote, clinozoisite and opaque minerals). Muscovite is abundant as buckled detrital grains, generally subparallel to bedding. This preferred orientation S_2 most probably represents the record of the deformation phase D_2, but it may also represent a "sedimentary cleavage" that formed due to a preferential orientation of mica during sedimentation. The main schistosity S_3 is defined partly by reoriented detrital muscovite and partly by more fine-grained muscovite that is interpreted as the product of recrystallization of the original detrital pelitic fraction during the main metamorphism M_3. Detrital muscovite is often observed as intergrowths with chlorite. The crystallization of chlorite can not directly be related to the formation of S_3. Consequently, it is not clear, if chlorite crystallized during M_3 or during an earlier stage of metamorphic crystallization that could have been related to D_2.

Upper chlorite zone

Sedimentary bedding still dominates the aspect of the Phe Formation in the upper chlorite zone. Sedimentary structures, however, are rarely preserved. The metapelites consist of slates displaying components of detrital quartz, K-feldspar and plagioclase in a matrix generally made up of muscovite, chlorite and locally also of graphite, that define the main schistosity S_3. During the main metamorphism M_3 fine-grained muscovite grew coarser from NE to SW and detrital muscovite mostly recrystallized. The grain size of chlorite also increases considerably from NE to SW. S_2 is preserved as rare relics marked by muscovite and chlorite within quartz layers (Fig. 6b). By contrast with the oldest schistosity in the lower chlorite zone, these S_2 relics are considered to definitely document the existence of the deformation D_2 and the metamorphism M_2 in the upper chlorite zone as they are unlikely to represent a sedimentary cleavage.

The stability of the M_2/M_3 assemblage chlorite + K-feldspar in the chlorite zone is limited by reaction (1) in the KFMASH system. The P-T region corresponding to this assemblage is not certain, maximum temperatures ranging between $T \approx 300$ and 400 °C (Fig. 5).

3.1.2. Biotite zone

In the biotite zone the Phe Formation metapelites are slates and phyllites that differ from the upper chlorite zone slates by the presence of additional biotite on the main schistosity S_3, indicating that M_3 reached biotite zone conditions in this area. Relics of S_2 within quartz layers by contrast are free of biotite. Accordingly, the main metamorphism M_3 reached biotite zone conditions, whereas M_2 did not exceed chlorite zone conditions.

The first appearance of biotite in low-Al pelites is defined by reaction (1) in the KFMASH system, the location of which is most likely between $T \approx 300$ and 400 °C (Fig. 5).

3.1.3. Garnet zone

In the garnet zone the metapelites are mainly phyllites, two-mica schists and biotite schists with additional garnet. The sedimentary bedding is well preserved on all scales, the main schistosity is S_2. The rocks consist of quartz, plagioclase, biotite, muscovite, chlorite and garnet poikiloblasts. Locally, graphite is abundant. The main schistosity S_2 as well as S_3 and relics of S_1 are marked by biotite, muscovite and chlorite (Fig. 6c). Garnet is on one hand wrapped around by S_2 in an augen-like texture, documenting its existence prior to S_2, on the other hand it overgrows S_1, establishing that it crystallized post-D_1 and pre-or syn-D_2. As a consequence, garnet growth is considered to be related to both stages of metamorphic crystallization M_1 and M_2, indicating that both of them reached garnet zone conditions in this area. By contrast, no garnet growth related to S_3 is observed. It is, however, important to note that garnets do not show any signs of resorption. This may indicate that the M_3 metamorphic conditions were also within or very close to the stability of garnet.

The stability of the main M_2 mineral assemblage garnet + biotite + chlorite + muscovite + quartz is limited by the reactions (2) and (4) in the MnKFMASH system (for X_{sps} up to 0.2, the maximum content measured in the analyzed garnets), constraining the temperature between $T \approx 460$ and 600 °C (Fig. 5). The discontinuous reaction (2) implies that garnet should crystallize consuming biotite and chloritoid. However, as no chloritoid occurs in the low-Al pelites of the biotite zone,

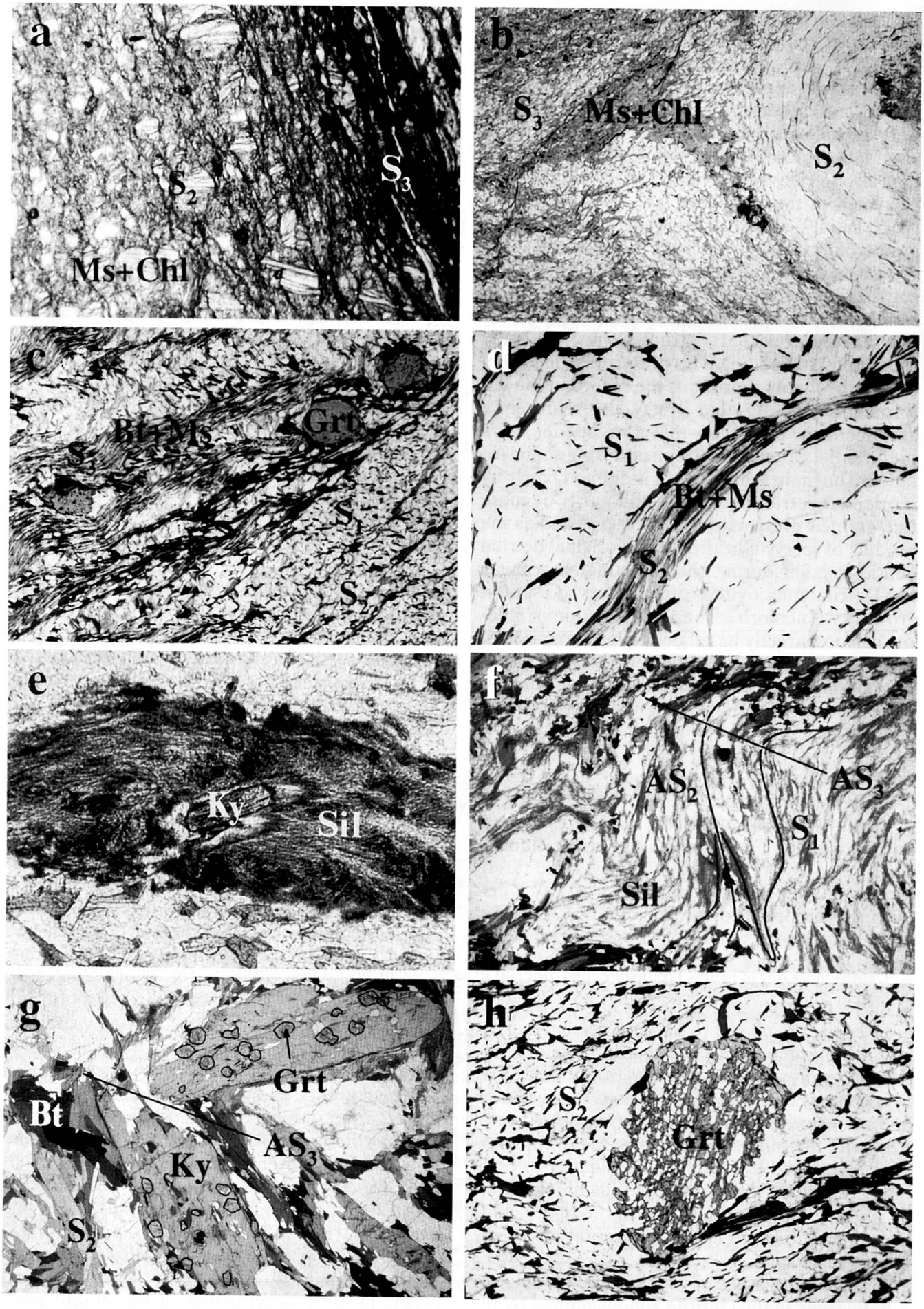
a
S3
S2
Ms+Chl
b
S3
Ms+Chl
S2
c
Bt+Ms
Grt
S3
S1
S2
d
S1
Bt+Ms
S2
e
Ky
Sil
f
AS2
AS3
S1
Sil
g
Grt
Bt
AS3
Ky
S2
h
S2
Grt

this reaction is unlikely to account for the formation of garnet. Garnet is more likely to have formed by the continuous reaction chlorite + quartz + muscovite = garnet + annite + H_2O. The P-T conditions of this reaction depend on the mineral compositions in the KFMASH system and therefore, it does not show up in the grid in figure 5.

3.1.4. Kyanite zone

This zone is referred to as the kyanite zone because over 90% of the rocks display the kyanite zone M_2/M_3 metamorphic mineral assemblage. However, the M_{1b} and M_4 sillimanite-bearing mineral assemblages also occur in this zone. In plate 1, the occurrence of M_4 sillimanite in the Tos Dextral Transtension Zone is indicated. The metapelites in the kyanite zone are generally medium- to coarse-grained garnet-bearing two-mica gneisses and schists with additional kyanite and/or sillimanite, consisting of quartz, plagioclase, biotite, white mica, garnet, kyanite, sillimanite, tourmaline and rare K-feldspar. Staurolite, apatite, rutile, ilmenite, zircon and monazite are accessories. These rocks display a strong metamorphic mineral segregation separating quartz- and plagioclase-rich microlithons from biotite- and muscovite-rich cleavage domains that represent the main schistosity S_2 (Fig. 6d). Relics of S_1 occur within the microlithons and in quartz layers, defined by biotite and muscovite. Locally, in mica-rich layers, a S_3 schistosity occurs that is also defined by biotite and muscovite. The primary sedimentary bedding is indicated by variable mineral ratios. Kyanite and/or sillimanite are abundant only in a few beds that constitute about 5% of the Phe Formation paragneisses. In the remaining 95%, aluminosilicates are rare.

The first stage of metamorphic crystallization M_{1a} is represented by relics of kyanite in the center of aggregates of fibrolitic sillimanite that are oriented parallel to S_1 (Fig. 6e). M_{1a} is therefore interpreted to be related to an early stage of D_1 that reached kyanite zone conditions. The second stage of metamorphic crystallization M_{1b} is characterized by the mineral assemblage biotite, muscovite and locally fibrolitic sillimanite on S_1 (Fig. 6f). Relics of K-feldspar frequently occur in samples in which S_1 is preserved. The M_{1b} mineral assemblage biotite + muscovite + sillimanite ± K-feldspar indicates conditions close to the vapor-absent melting reactions (10 and 11 in figure 5) and between the kyanite = sillimanite (12) and sillimanite = andalusite (14) equilibria. This limits the temperature range between T ≈ 620 and 760 °C, and pressure may have attained 900 MPa.

The third stage of metamorphic crystallization M_2 is related to the main schistosity S_2. S_2 is marked by biotite and muscovite (Fig. 6d) and locally by kyanite crystals several centimeters long (Fig. 6g) that define the mineral stretching lineation L_2. Chlorite is absent on S_2. Garnet poikiloblasts with inclusions of S_2 marked by biotite, muscovite, quartz and plagioclase indicate syntectonic growth with respect to S_2 (Fig. 6h). Staurolite is rare in the studied area. It was found as small relics on S_2 (Fig. 7a) and as inclusions in D_2-syntectonic garnet. Associated with M_2, small quantities of leucosomes formed, that consist of quartz, plagioclase and rare K-feldspar (Fig. 7b). As these melts rarely migrated more than half a meter, they are considered to represent in-situ melting of the metapelites. The M_2 assemblage plagioclase ($X_{An} \approx 20$) + quartz + biotite + muscovite + garnet + kyanite + melt ± staurolite indicates metamorphic conditions within the kyanite zone for M_2, its stability being limited by the reactions (6), (8) and (9) as well as by the kyanite = sillimanite equilibria (12) in figure 5, defining a P-T range of T ≈ 640–720 °C and P ≈ 600–1100 MPa. The widespread presence of small quantities of melt implies a temperature above the vapor-saturated melting reaction (7), that is, above T ≈ 650 °C.

During the fourth stage M_3, minor mineral growth is documented. Biotite and muscovite on S_2 were crenulated during D_3 and locally they form a schistosity S_3. Occasionally, small kyanite

← *Fig. 6* Textural and structural relationships. The scale given within brackets corresponds to the long dimension of the image, SW is to the left hand side. All photomicrographs are from Phe Formation metapelites.
(a) Slate from the lower chlorite zone. S_2 is defined by muscovite intergrown with chlorite and S_3 is defined by fine-grained muscovite [1.5 mm]. (b) Phyllite from the upper chlorite zone showing a F_2 fold. S_2 and S_3 are defined by muscovite and chlorite [5 mm]. (c) Schist from the garnet zone, showing the schistosities S_1 and S_2 in the competent layer on the right hand side and S_2 and S_3 in the incompetent layer on the left hand side [9.5 mm]. (d) Crenulation cleavage S_2, marked by biotite and muscovite, overprinting S_1 that is preserved in microlithons [13.5 mm]. (e) Kyanite surrounded by aggregates of fibrolitic sillimanite [1.5 mm]. (f) Fibrolitic sillimanite on S_1, folded by F_2 and F_3, that form a convergent-divergent interference pattern [18.5 mm]. (g) Kyanite on S_2, broken by F_3 folding. Kyanite contains small garnet inclusions that may represent relics of M_1 [18 mm]. (h) D_2-syntectonic garnet, containing S_2 [16 mm]. (d)–(h) are schists and gneisses from the kyanite zone.

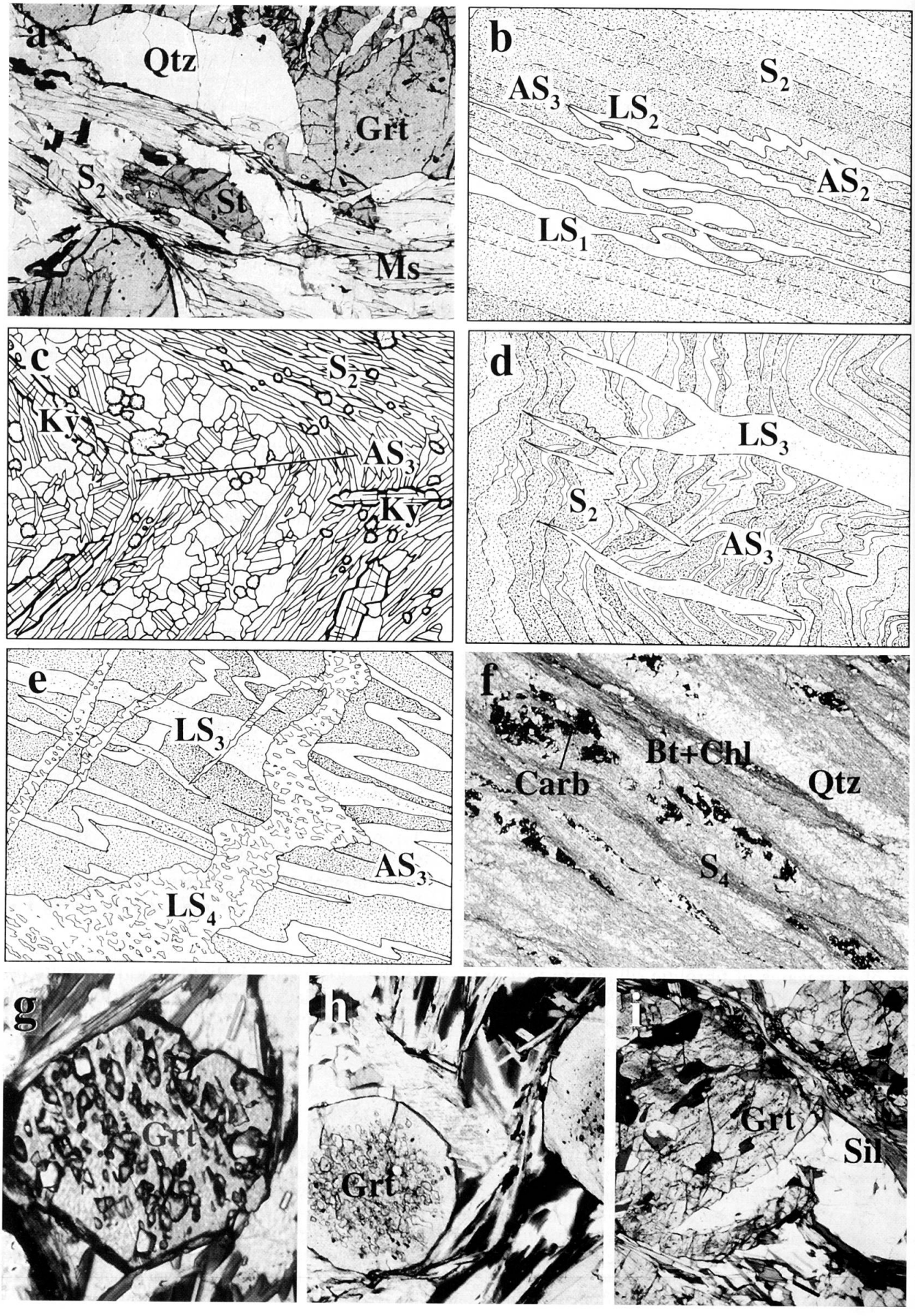
a
Qtz
Grt
S_2
St
Ms
b
AS_3
LS_2
S_2
AS_2
LS_1
c
S_2
Ky
AS_3
Ky
d
LS_3
S_2
AS_3
e
LS_3
AS_3
LS_4
f
Carb
Bt+Chl
Qtz
S_4
g
Grt
h
Grt
i
Grt
Sil

crystals grew parallel to the axial surface of F_3 folds (Fig. 7c). Broken kyanites on S_2 are a common feature in F_3 fold hinges (Fig. 6g). Leucosomes that are oriented parallel to F_3 axial surfaces are interpreted to represent in-situ melting during M_3 (Fig. 7d). Although little mineral growth is documented during M_3, the presence of kyanite on S_3 and migmatization indicate conditions in the same range as for M_2.

During both M_2 and M_3, small quantities of leucosomes formed, that are interpreted to be the result of vapor-saturated melting. This indicates that during M_2, not all vapor was consumed. This feature is noteworthy and may indicate that M_3 represents the direct continuation of M_2 metamorphic conditions during D_3.

The fifth stage of metamorphic crystallization M_4 is related to D_4 transtension in the Tos Dextral Transtension Zone (Figs 1, 2 and plate 1). It is characterized by fibrolitic sillimanite intergrown with biotite on D_4 shear bands (Fig. 3, inset a). Kyanite is crosscut by sillimanite and partly resorbed, indicating that sillimanite was the stable aluminosilicate during M_4. D_2 and D_3 structures are crosscut by leucosomes representing migrated melts (Fig. 7e). This indicates local, but intensive melt formation after D_3 and therefore most probably during M_4. Consequently, the vapor-absent melting reaction (10) was crossed during M_4, which restricts the P-T range to above $T \approx 720$ °C and below $P \approx 820$ MPa. This implies that the staurolite-consuming reaction (8) was also crossed during M_4, which is consistent with the rare occurrence of staurolite in the form of strongly resorbed crystals.

3.1.5. Zone of retrograde greenschist facies metamorphism

In a zone 2–2.5 km wide at the base of the High Himalayan Crystalline, the kyanite zone mineral assemblage in the Phe Formation pelites was retrogressively overprinted by a greenschist facies metamorphism related to D_4 thrusting with a top-to-the SW shear sense along the Main Central Thrust (Fig. 3).

In general, the rocks are more fine-grained, K-feldspar is lacking, muscovite is more abundant and kyanite was transformed to muscovite during retrogression (Fig. 3, inset b). D_4 thrusting is concentrated in shear zones, the frequency and intensity of which is strongest at the base of the High Himalayan Crystalline. These shear zones are characterized by C- and C'-type shear bands that overprint S_2 and that are marked by biotite and chlorite, defining the schistosity S_4 (Fig. 3, inset c). In D_4 shear zones, chlorite replaced biotite on S_2 and garnet rims were transformed to chlorite (Fig. 3, inset c).

3.2. LESSER HIMALAYAN SEQUENCE

In the Lesser Himalayan Sequence, D_4 thrusting is concentrated in a zone about 2 km wide in the calcschists and phyllites of the mélange zone below the base of the Crystalline Nappe and in thin layers of schists and phyllites within the underlying massive Berinag Quartzite (Fig. 3). The mineral content of these rocks is variable, the calcschists consisting of calcite, dolomite, quartz, muscovite, chlorite, biotite, graphite, opaque minerals, detrital sericitized plagioclase and K-feldspar (Fig. 7f). Detrital tourmaline and zircon are accessory minerals. The schists and phyllites are made up of muscovite, chlorite, biotite, graphite and ribbons of equigranular-polygonal quartz. D_4 thrusting is indicated by C- and C'-type shear bands marked by muscovite, biotite and chlorite, forming S_4 that overprints all earlier structures. Locally, S_4 is very strong and represents the main schistosity (Fig. 7f). The assemblage chlorite + biotite in the schists and phyllites is defined by reaction (1) in the KFMASH system, the location of which is most likely between $T \approx 300$ and 400 °C (Fig. 5).

4. Thermobarometry

Despite the complex tectonometamorphic evolution of the studied section, the major metamorphic minerals observed can either be assigned to the stage of metamorphic crystallization M_2 in the

← *Fig. 7* Textural and structural relationships. The scale given within brackets corresponds to the long dimension of the image, SW is to the left hand side. (a)–(e) and (g)–(i) are pelitic Phe Formation schists and gneisses. (a)–(e) and (h), (i) are from the kyanite zone. (a) Relic of staurolite on S_2 [8 mm]. (b) LS_2 leucosomes oriented parallel to S_2 that formed during F_2 folding and M_2 metamorphism. S_2 and LS_2 were subsequently folded by F_3 folds. The leucosomes folded by F_2 folds (LS_1) most probably formed during M_1 [40 cm]. (c) S_2 schistosity folded by F_3 folds. Kyanite occurs on S_2 and parallel to the axial surface of F_3 [15 mm]. (d) LS_3 Leucosomes oriented parallel to the axial surface of F_3 folds, related to D_3/M_3 [55 cm]. (e) LS_4 leucosomes crosscutting F_3 folds, related to D_4/M_4 [65 cm]. (f) Calcschist from the mélange zone on top of the Berinag Quartzites; S_4 is the main schistosity [9 mm]. (g) Euhedral garnet from a garnet zone schist [1 mm]. h) Euhedral garnets from a kyanite zone gneiss [3 mm]. (i) Resorbed garnets from a kyanite zone gneiss, crosscut by sillimanite on a SB_4 shear band [5.5 mm].

garnet and kyanite zones, to M_3 in the chlorite and biotite zones or to M_4 in the Main Central Thrust Zone. In the kyanite zone this is documented by D_2-syntectonic garnet growth and by biotite, muscovite and kyanite defining S_2. In these rocks textural relationships suggest equilibrium between

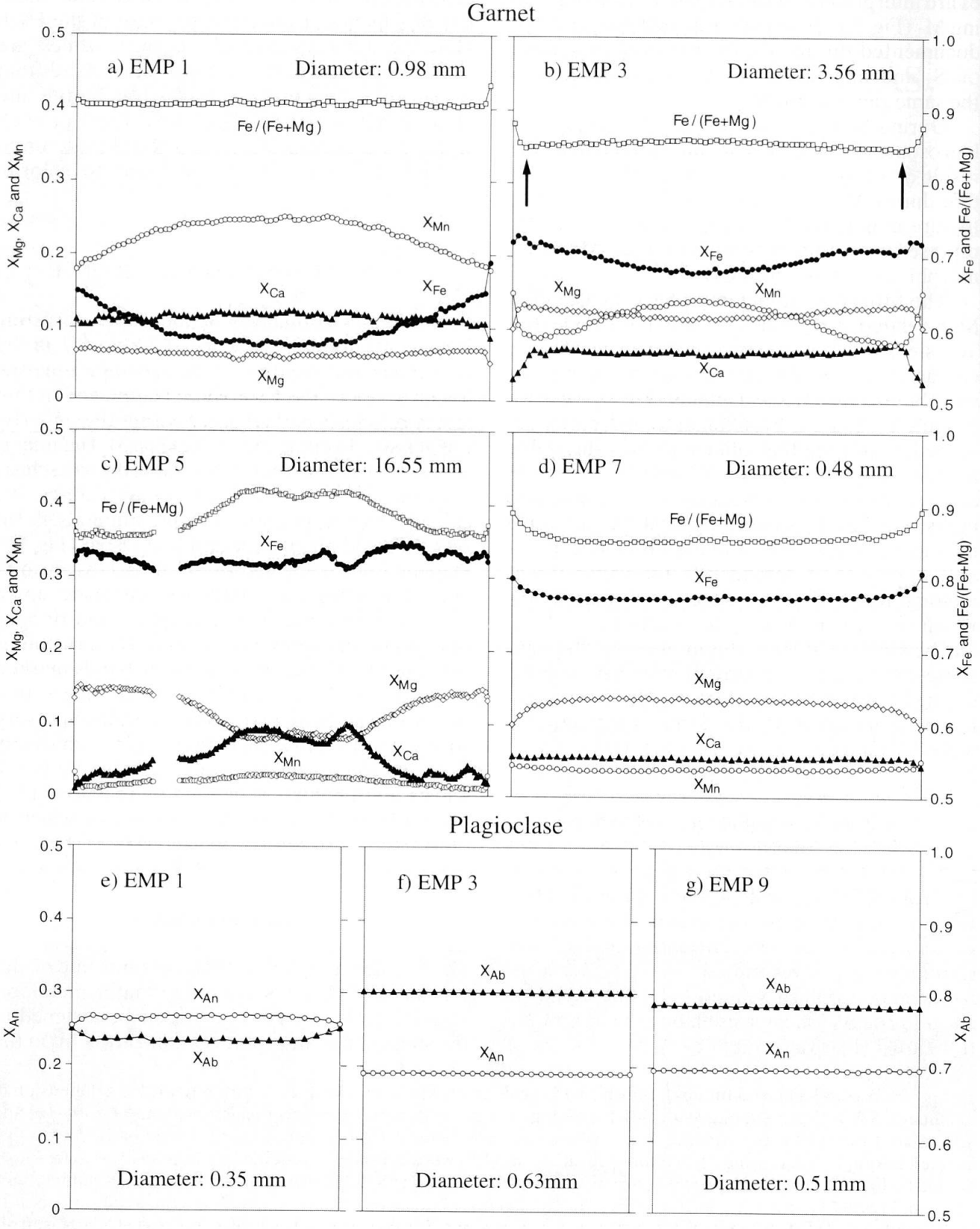

Fig. 8 Representative zoning profiles in garnet and plagioclase from metapelites in the Spiti valley–eastern Lahul-Parvati valley transect. EMP 1 is from the garnet zone, EMP 3, 5, 7 and 9 are from the kyanite zone. Arrows in (b) indicate the Fe/(Fe + Mg) minimum. See figure 9 for sample locations.

the major phases garnet, biotite, muscovite, plagioclase, quartz and kyanite during M_2. This allows the application of garnet–biotite (GARB) thermometry as well as garnet–aluminosilicate–quartz–plagioclase (GASP) and garnet–biotite–muscovite–plagioclase (GMAP) barometry to quantify the equilibrium P-T conditions during M_2 throughout the High Himalayan Crystalline. Analytical procedure and mineral compositions are given in the Appendix.

4.1. MINERAL ZONING PROFILES

To characterize the zoning in garnet and plagioclase, the two most typical minerals for fractional crystallization during progressive metamorphism, compositional traverses have been measured in all samples analyzed for thermobarometry.

4.1.1. Garnet zoning

Growth zoning

Garnets from the garnet zone show slightly bell-shaped compositional profiles characterized by a core to rim X_{Fe} increase, revealing a typical growth zoning (Fig. 8a). Such a growth zoning is interpreted to represent a sequence of equilibrium compositions adapted to increasing P-T conditions during garnet growth. A similar zoning is shown by garnets of > 1 mm diameter from the kyanite zone (Fig. 8b). With increasing diameter, zoning in these garnets becomes stronger, the most extreme example occurring in an extraordinarily large garnet of 16.5 mm diameter (Fig. 8c). This large garnet shows a strong bell-shaped zoning with a core to rim X_{Fe} and X_{Mg} increase and parallel X_{Ca} and Fe/(Fe + Mg) ratio decrease. The abrupt change in composition after 1/3 of the radius may reflect the effect of the garnet-consuming NCKFMASH reaction garnet + chlorite + muscovite = staurolite + biotite + plagioclase + quartz + H_2O. Small size garnets (< 1mm diameter) from the kyanite zone, by contrast, show rather homogeneous compositional profiles (Fig. 8d). The change in the strength of zoning from small size garnets to large size garnets in the kyanite zone is interpreted to indicate a homogenization of the garnet composition through diffusion at high temperatures that progressed from rim to core. As a consequence, small garnets were entirely homogenized whereas the core composition of large garnets was only slightly modified or even entirely preserved.

Retrograde zoning

Retrograde zoning in garnet is generally considered as the result of either a Fe–Mg exchange reaction involving garnet and biotite or both a Fe–Mg exchange reaction and a net transfer reaction. Exchange reactions cause only a change in the composition of minerals and do not affect the modal proportions of the phases involved. As a consequence, garnet crystals maintain their euhedral shape. In high-grade metamorphic pelites in the KFMASH system, garnet + K-feldspar + H_2O = sillimanite + biotite + quartz is the possible net transfer reaction (SPEAR, 1993). This reaction consumes garnet and accordingly, garnet crystals should show resorbed rims.

Throughout the garnet and kyanite zones, the garnets systematically show an increase in Fe/(Fe + Mg) ratio towards the rims, indicating Fe–Mg exchange between garnet and biotite during cooling. This increase is strongest where garnet is in direct contact with biotite. From the garnet zone to the kyanite zone, the penetration of Mg and Fe diffusion increases as a function of the increasing equilibration temperature (Fig. 8a vs Figs 8b–d). Garnets from the garnet zone always show euhedral grain boundaries (Fig. 7g), whereas in the kyanite zone, both euhedral garnets and garnets with resorbed rims occur (Figs 7h, i), indicating that in the kyanite zone the above net transfer reaction may be of a certain importance during retrogression. In fact, most of the resorbed garnets occur in the Tos Dextral Transtension Zone, where D_4 sillimanite- and biotite-bearing extensional shear bands occur and where the rocks are nearly K-feldspar-free.

4.1.2. Plagioclase zoning

Compositional profiles of plagioclase show no zoning except for garnet zone plagioclases. (Figs 8e–g). Cation diffusion in plagioclase is very slow (GROVE et al., 1984) and once plagioclase is produced, it cannot easily change composition during retrograde equilibration. Consequently, these homogeneous profiles indicate that plagioclase grew with a stable composition in the kyanite zone.

4.2. ESTIMATES OF APPARENT PEAK P-T CONDITIONS

Both net transfer and exchange reactions during cooling have a strong influence on the composition of garnet and biotite crystals, specifically on the Fe/(Fe + Mg) ratio. Consequently, as the GARB thermometer is particularly sensitive to

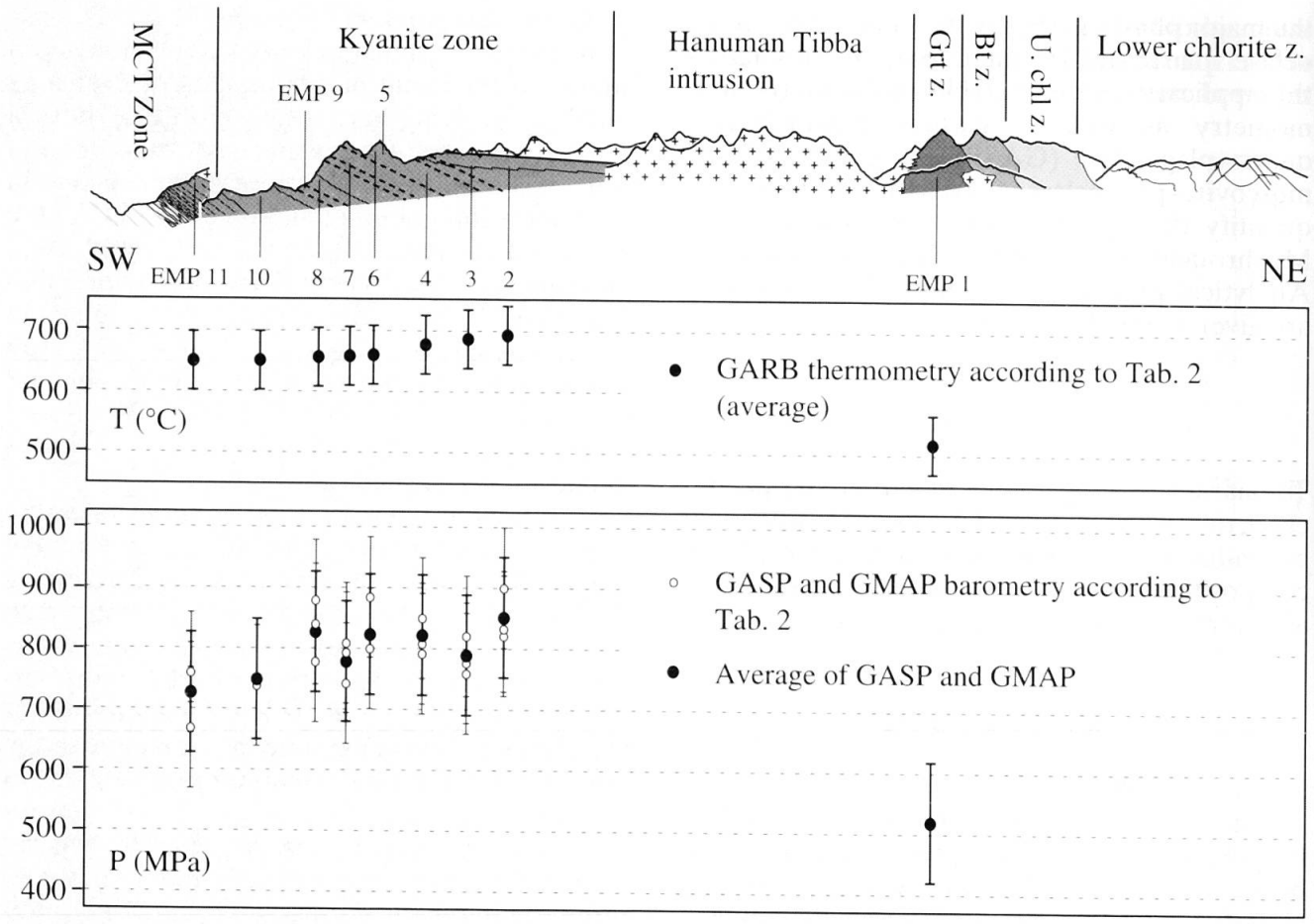

Fig. 9 Pressure and temperature profiles for the Spiti valley–eastern Lahul-Parvati valley transect, based on the results presented in table 2. The section is a reduction in size of plate 1.

the Fe/(Fe + Mg) ratio, temperature estimates based on GARB thermometry do not represent peak temperatures and are therefore referred to as apparent temperatures. In the case of exchange reactions only, the estimated temperature will be lower than the peak temperature and in the case where both exchange and net transfer reactions can operate, thermometry will yield a temperature that is higher than the peak temperature (SPEAR, 1991; SPEAR and FLORENCE, 1992; SPEAR, 1993).

To minimize the influence of retrograde reactions for the estimation of peak temperatures, garnet compositions with the smallest possible Fe/

Tab. 2 Summary of thermobarometry results. EMP 1 is from the garnet zone, EMP 2 to EMP 10 are from the kyanite zone and EMP 11 is from the zone of retrograde greenschist facies metamorphism (Main Central Thrust Zone). See figure 9 for sample locations.

	Apparent peak P–T estimates						**Rim T estimates**
	GARB (HODGES and SPEAR, 1982) GASP (HODGES and SPEAR, 1982)		GARB (HODGES and SPEAR, 1982) GASP (HODGES and CROWLEY, 1985)		GARB (HODGES and SPEAR, 1982) GMAP (HODGES and CROWLEY, 1985)		GARB (HODGES and SPEAR, 1982)
Sample	T (°C) ± 50	P (MPa) ± 100	T (°C) ± 50	P (MPa) ± 100	T (°C) ± 50	P (MPa) ±100	T (°C) ± 50
EMP 1	–	–	–	–	515	520	505
EMP 2	690	830	695	900	690	825	520
EMP 3	685	775	690	820	685	760	520
EMP 4	675	790	680	850	680	810	560
EMP 6	660	800	665	880	660	800	540
EMP 7	660	740	665	810	665	790	550
EMP 8	730	780	635	880	635	840	540
EMP 9	–	–	–	–	–	–	535
EMP 10	650	750	650	750	650	740	520
EMP 11	650	760	650	760	645	670	530

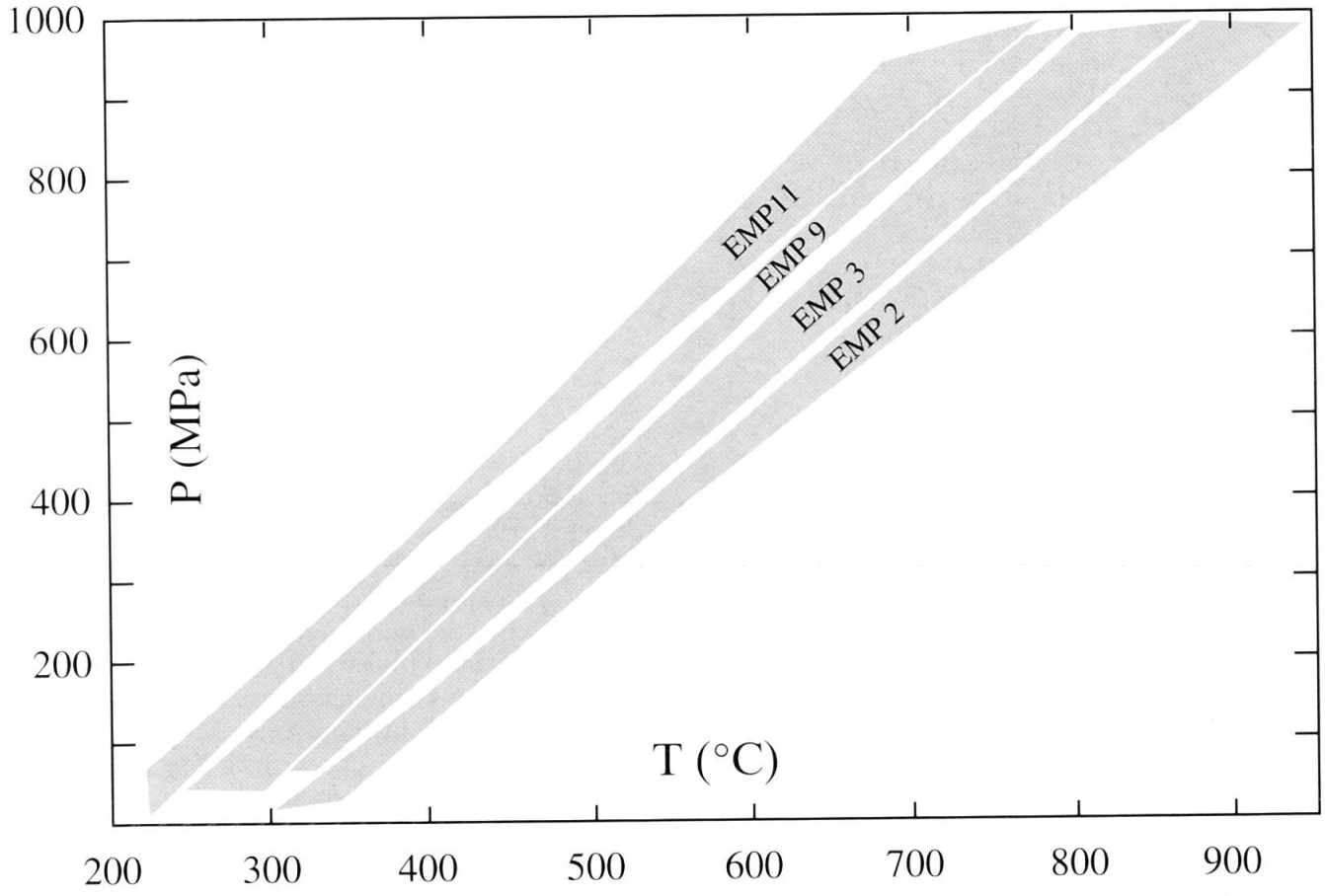

Fig. 10 Summary of GASP and GMAP reaction curves for rim barometry of four selected samples according to the calibrations of HODGES and SPEAR (1982) and HODGES and CROWLEY (1985), representing a semiquantitative approach to present the upsection decrease of pressure in the High Himalayan Crystalline during M_4 from sample EMP 11 to sample EMP 2. See figure 9 for sample locations.

(Fe + Mg) ratio near the rim were used for thermobarometry (indicated by arrows in figure. 8b). These compositions are suggested to be the closest possible to the compositions of the peak of metamorphism, as they were apparently not influenced by retrograde reactions yet.

Retrograde Fe–Mg exchange reduces and net transfer reactions enlarge the Fe/(Fe + Mg) ratio in biotite. However, as diffusion in biotite is rapid relative to cooling rates, the interior of the biotite crystals quickly equilibrate with the rim and biotite crystals remain homogeneous. As a consequence, it is not possible to control the effect of retrograde reactions on biotite. In all samples used, the quantity of garnet is very small with respect to biotite. Garnet therefore represents a small reservoir for cation exchange with biotite and accordingly, the effect of cation exchange between these two phases can be considered as small for biotite. Consequently, it is suggested that the influence of both types of retrograde reactions on biotite is negligible in the analyzed samples, and that the biotite compositions are close to peak compositions.

GASP and GMAP barometers are particularly sensitive to the Ca-content of garnet and plagioclase. The homogeneous compositional profiles of kyanite zone plagioclases indicate stable plagioclase composition during prograde growth. Consequently, in this special case, the plagioclase composition is treated as if it had been in equilibrium with every point in garnet and it is used to estimate the pressure at the Fe/(Fe + Mg) minimum. Ca diffusion in garnet is slow during retrograde equilibration with respect to Fe and Mg diffusion. Accordingly, the Ca-zoning is considered to represent the Ca-content during prograde garnet growth. During prograde growth on a "nappe formation" P-T path, X_{Ca} remains relatively stable and decreases during decompression only (SPEAR, 1993). In all garnet compositional profiles used for thermobarometry, X_{Ca} starts to decrease at a point that coincides with the Fe/(Fe + Mg) minimum. Therefore, X_{Ca} at the Fe/(Fe + Mg) minimum is suggested to represent the Ca-content near the peak of metamorphism, indicating that the estimated pressures may be close to peak pressures.

Apparent peak P-T estimates are summarized in table 2 and presented in figure 9 as a function of their structural position in the section. P-T results for aluminosilicate-bearing rocks obtained from two independent sets of thermobarometer (GARB-GASP and GARB-GMAP) and with two different calibrations for GARB-GASP (HODGES and SPEAR, 1982; HODGES and CROWLEY, 1985) generally overlap within error, suggesting that the analyzed mineral assemblages correspond to well-equilibrated systems.

Apparent peak P-T estimates from the garnet zone indicating a temperature of 515 °C and a pressure of 520 MPa fit the stability conditions deduced from the petrogenetic grid (I in figure 5). In the kyanite and MCT zones peak P-T conditions decrease slightly from the NE to the SW from T ≈ 690 °C and P ≈ 850 MPa to T ≈ 650 °C and P ≈ 730 MPa (II and III in figure 5). Samples that most probably underwent retrograde Fe–Mg exchange only and samples that underwent both Fe–Mg exchange and net transfer reaction fit within the same trend of apparent temperatures. This may indicate that the influence of the garnet-consuming net transfer reaction was small in the analyzed samples and, as a consequence, that the presented temperature estimates represent minimum values of true peak temperatures.

4.3. RIM P-T ESTIMATES

Rim P-T conditions have been estimated using garnet compositions from the outermost rims that are in contact with biotite. As all samples analyzed underwent at least retrograde Fe–Mg exchange, the estimated temperatures are expected to be higher than T ≈ 500 °C, that is the temperature at which Fe–Mg diffusion in garnet ceases to penetrate measurably (SPEAR and FLORENCE, 1992), and lower than the true metamorphic peak temperature (Tab. 2). As it is not known to what extent the analyzed samples were influenced by retrograde reactions, the presented rim temperatures may represent any mixture between the peak temperature and T ≈ 500 °C.

Barometry is less sensitive to the Fe/(Fe + Mg) ratio and therefore the results of rim barometry may represent true pressures attained during cooling. However, as the rim temperature estimates do not yield values that can be used to fix pressures on the GASP and GMAP reaction curves, a semiquantitative approach is selected to present the evolution of pressure. A comparison of the results of rim GASP and GMAP barometry for several High Himalayan Crystalline samples shows a decrease of the rim pressure towards the Tos Dextral Transtension Zone (Fig. 10). These results fit well with the structural model of the Crystalline Nappe that implies decompression by NE-directed normal movement in the Tos Dextral Transtension Zone (Figs 2, 3).

5. P-T Path

5.1. HIGH HIMALAYAN CRYSTALLINE

No tectonic discontinuities have been observed between the Barrovian mineral zones within the Tethyan Himalaya and the High Himalayan Crystalline. The mineral assemblages characterizing the various zones are therefore considered to be related to a continuous metamorphic evolution during M_2, M_3 and M_4.

Structural and microtextural observations imply that M_2 is the main metamorphism in the garnet and kyanite zones and that M_3 is the main metamorphism in the chlorite and biotite zones. In the garnet and kyanite zones M_3 played a less important part, as it represents a continuation of M_2 conditions, whereas in the chlorite and biotite zones, M_2 is only of minor importance. The chlorite and biotite zones are therefore mainly defined by M_3 mineral assemblages, whereas the garnet and kyanite zones are defined by M_2 assemblages including M_3 assemblages.

Petrographic features and P-T estimates allow constraints to be placed on the metamorphic evolution for garnet- and kyanite zone samples. On this basis, the P-T path during M_1 can be roughly constrained and a continuous P-T path from M_2 to M_4 can be drawn for the High Himalayan Crystalline.

The oldest observed metamorphic event M_1 is characterized by relics of kyanite (M_{1a}) in the center of aggregates of fibrolitic sillimanite that occur together with the mineral assemblage biotite + muscovite ± K-feldspar (M_{1b}). Most probably, a small quantity of melt was generated during M_1 as indicated by leucosomes deformed by F_2 folds (Fig. 7b). This indicates that during M_1, the kyanite = sillimanite reaction (12 in figure 5) was crossed close to the vapor-absent melting reactions (10 and 11). Arrow A in figure 5 indicates the transition from stage M_{1a} to stage M_{1b}. The exact position and dP/dT slope of arrow A, however, cannot be determined.

The stability conditions deduced from the petrogenetic grid for the M_2 garnet zone mineral assemblage are limited by the reactions (2) and (4) in figure 5. They coincide with the P-T estimates of garnet zone sample EMS 1, which represents the starting point of the M_2 to M_4 P-T -path

(I in figure 5). In the M_2 kyanite zone mineral assemblage chlorite is completely resorbed and small quantities of migmatites occur, representing in-situ melting related to M_2. Together with a systematic presence of plagioclase in kyanite-bearing assemblages, this implies a prograde path below reaction (9) and crossing reaction (6) and (7) in the kyanite stability field (Fig. 5, arrow B1). This fits well with the maximum P-T estimates for the samples EMP 2 and EMP 8 (II in figure 5). It is suggested that the M_2 peak metamorphic conditions did not cross the vapor-absent melting reaction (10), because only small amounts of melt formed during M_2. The M_3 mineral assemblage indicates that the metamorphic crystallization during M_3 was a direct continuation of M_2 under similar conditions but with minor mineral growth.

In the Tos Dextral Transtension Zone M_2 kyanite crystals were cut by D_4 shear bands marked by M_4 sillimanite and biotite. Migmatites representing migrated melts crosscut D_2 and D_3 structures, suggesting local, but intensive melt formation posterior to D_3 and therefore most probably during M_4. Staurolite occurs as rare relics only, and garnet recorded decompression after passing the pressure peak of metamorphism as indicated by Ca zoning and by rim barometry, implying that garnet continued to crystallize, whereas staurolite was consumed. These features suggest a decompressive path crossing the staurolite-consuming reaction (8) and the vapor-absent melting reaction (10) close to the Ky = Sil equilibria (12) during D_4 extension (Fig. 5, arrow B2). Crossing of reaction (10) implies the formation of K-feldspar. This mineral, however, is rare in the kyanite zone pelites and, if it occurs, it is strongly resorbed. This could indicate that K-feldspar was consumed by the retrograde reaction garnet + K-feldspar + H_2O = sillimanite + biotite + quartz that is suggested to have operated during retrogression. Decompression after the peak of metamorphism increases in the Tos Dextral Transtension Zone from the SW to the NE (Fig. 10). The maximum amount of decompression, however, cannot be estimated as no quantitative constraints were obtained from the analyzed samples.

Towards the base of the High Himalayan Crystalline, in the zone of retrograde greenschist facies metamorphism, the M_2 stability conditions are given by the presence of garnet, kyanite and small quantities of M_2 leucosomes, indicating that reaction (7) was crossed above reaction (12) during M_2 (Fig. 5, arrow C1). The M_2 peak P-T estimates are slightly lower than in the center of the nappe (III in figure 5). Sillimanite, K-feldspar and leucosomes representing migrated M_4 melts do not occur, implying that the reactions (10) and (12) were not crossed after the peak of metamorphism in this part of the section. The widespread presence of biotite and chlorite on shear bands related to D_4 SW-directed thrusting as well as chlorite overgrowing garnet rims and muscovite replacing kyanite in the zone of retrograde greenschist facies metamorphism indicate that the metamorphic conditions decreased to biotite zone conditions during D_4 thrusting of the High Himalayan Crystalline over the Lesser Himalayan Sequence (Fig. 5, arrow C2).

5.2. LESSER HIMALAYAN SEQUENCE

During D_4 thrusting the calcschists and phyllites of the mélange zone and thin layers of schists and phyllites within the massive Berinag Quartzite reached M_4 biotite zone metamorphic conditions similar to M_4 conditions at the base of the overlying Crystalline Nappe. It cannot be excluded that the Lesser Himalayan Sequence rocks were already metamorphic prior to M_4. The conditions of this metamorphism, however, did not exceed M_4 conditions. Consequently, the Lesser Himalayan Sequence rocks followed a prograde P-T path during D_4 thrusting in the Main Central Thrust Zone (Fig. 5, arrow D). Because the P-T conditions of the greenschist facies metamorphism in the Main Central Thrust Zone cannot be determined precisely, the arrows C2 and D are poorly constrained and should be considered as purely qualitative.

6. Discussion

6.1. METAMORPHISM M_1

Well preserved relics of a strong S_1 schistosity and rare isoclinal F_1 folds within the High Himalayan Crystalline in the garnet- and kyanite zones indicate that D_1 was an important phase of deformation. However, due to the subsequent D_2, D_3 and D_4 overprint, no information about the vergence and the orientation of fold axes and axial surfaces of F_1 folding is preserved and therefore, D_1 deformational conditions are poorly known.

The most important information about D_1 comes from the $M_{1a/b}$ metamorphic mineral assemblages in the Phe Formation metapelites (Plate 1), indicating kyanite zone conditions in the Tos valley area during M_{1a}. This is in agreement with metamorphic conditions deduced from M_1 corona textures overprinting the magmatic mineral assemblages in rare olivine gabbro bodies that occur in the lowermost kyanite zone Phe For-

mation rocks in the Tos valley (WYSS and HERMANN, subm.). For these orthopyroxene + clinopyroxene + garnet + amphibolite + spinel coronas, peak conditions of T ≈ 700 °C and P ≈ 800–1000 MPa have been determined. During M_{1b}, sillimanite formed on S_1, indicating a change of the metamorphic conditions to the sillimanite zone. As the subsequent M_2 metamorphism was prograde, reaching kyanite zone peak conditions in the Tos valley, M_{1a}–M_{1b} are interpreted to represent an independent metamorphic cycle. Therefore, D_1 was an independent tectonometamorphic event that occurred prior to the NE-verging D_2 stacking of the Shikar Beh Nappe (WYSS et al., 1999). The Shikar Beh Nappe has for a long time been considered to be the first record of tectonic activity in the Himachal Himalaya (STECK et al., 1993, 1999; VANNAY, 1993; VANNAY and STECK, 1995).

Several authors found indications for pre-Himalayan orogeny. POGANANTE and LOMBARDO (1989) reported metabasites with relics of a granulite facies metamorphism from Zanskar and Lahul, and WALKER et al. (1999) found relics of an old metamorphism in the Zanskar area that are interpreted to be of pre-Himalayan age. ARGLES et al. (1999) discovered garnets with Sm–Nd ages >500 Ma in the Garwhal Himalaya and outside the NW Himalaya, FERRARA (1983) reported a 449±56 Ma Rb/Sr age on paragneisses from the Mt. Everest area. The predominating arguments for a pre-Himalayan event, however, are based on the sedimentary record showing several angular unconformities and sedimentation gaps. A prominent angular unconformity between the Lower Cambrian Karsha Formation and the Middle Ordovician Thaple Formation (Tab. 1) is interpreted as an exposure to erosion and continental clastic resedimentation due to the uplift of a Cambro-Ordovician mountain belt that may be related to Pan-African orogeny (GARZANTI et al., 1986; GAETANI and GARZANTI, 1991; VALDIYA, 1995). Some authors invoke that the concurrence of Cambro-Ordovician magmatic activity and exposure to erosion is the strongest argument for pre-Himalayan orogeny (SAXENA, 1980; GARZANTI et al., 1986). PANDE and SAXENA (1968), SAXENA (1973) and FUCHS (1992) interpreted sedimentary gaps as the evidence for Caledonian and Hercynian orogeny. JAIN et al. (1980) remain more general and invoke late Paleozoic epeirogenic movements.

If these unconformities are interpreted to represent erosion of an orogenic belt, it is expected that the structural and metamorphic record below and above the unconformities should indicate pre-erosional deformation and/or metamorphism. In other words, in such a case below the unconformity, at least one phase of deformation and/or one stage of metamorphic crystallization more should be observed than above the unconformity. Such a feature, however, has not been described until now. It is therefore suggested that these arguments should be treated with caution.

All these observations and their interpretations show that the existence of a pre-Himalayan orogeny is subject to investigation for a long time, but there is little consensus as to what the age of such an event could be. In the Phe Formation metapelites, M_1 overprints the hornfelsic contact aureole of the 495 ± 16 Ma old Hanuman Tibba intrusion (Rb/Sr whole rock isochron, dated by FRANK et al., 1977), indicating that M_1 must be younger than this intrusion (WYSS et al., 1999). As a consequence, D_1 may be considered as a pre-Himalayan or as an early Himalayan event.

6.2. METAMORPHISM M_2

In the High Himalayan Crystalline, structural and textural observations allow the peak P-T conditions during Tertiary Himalayan nappe stacking to be assigned to the stage of metamorphic crystallization M_2 that is related to formation of the NE-verging Shikar Beh Nappe. This feature has only been reported from the central and northern Himachal Himalaya until now (EPARD et al., 1995, STECK et al., 1999; WYSS et al., 1999). In the other part of the Himalayan orogen, peak P-T conditions are reported to be related to SW-directed nappe stacking (e.g. VANNAY and GRASEMANN, 1998 and references therein).

During the Barrovian-type M_2 metamorphism, the High Himalayan Crystalline rocks followed a prograde P-T path that reached different peak P-T conditions according to the tectonostratigraphic depth (Plate 1, Fig. 9). A prograde P-T path for M_2 is also supported by prograde mineral zoning in M_2 amphiboles from olivine gabbro bodies (WYSS and HERMANN, subm.). This indicates that M_2 represents an independent metamorphic stage and cannot be considered as a retrograde stage of M_1. It is important to note that the peak P-T conditions decrease downsection from the NE to the SW in the kyanite zone (Figs 5, 9), indicating an inverted zonation of M_2 isotherms and isobars. This feature will be discussed in the last section.

The NE-verging D_2 Shikar Beh Nappe is documented by S_2 and F_2 folds in the garnet zone, in the kyanite zone and in the zone of retrograde greenschist facies metamorphism along the Main Central Thrust, but by relics of S_2 solely in the biotite zone. In the chlorite zone D_2 is not clearly

documented. In the garnet- and kyanite zones M_2 is the main metamorphism, whereas in the biotite zone M_3 is the main metamorphism. At the transition between the garnet- and biotite zones, the M_2 metamorphic conditions decrease abruptly from garnet zone conditions to chlorite zone conditions (Plate 1). NE of this boundary the metamorphic zoning is the result of M_3 and SW of this boundary it is the result of M_2, M_3 being of subordinate importance. The abrupt decrease in the intensity of M_2 and S_2 and the disappearance of F_2 folds between the garnet- and biotite zones could be interpreted to represent the front of the NE-verging Shikar Beh Nappe. This assumption, however, requires the record of a large-scale thrust zone between the garnet zone and the biotite zone, a feature that is not documented in the field. STECK et al. (1998) interpreted a NE-directed thrust in the Lagudarsi La area NE of Spiti valley as a frontal thrust of the Shikar Beh Nappe. This may explain, why in the chlorite zone a schistosity S_2 occurs prior to the main schistosity S_3. However, if the nappe front is assumed to be situated more than 20 km to the NE, F_2 folds are not expected to disappear NE of the garnet zone to biotite zone boundary. Alternatively, the sudden decrease of M_2 metamorphic conditions could reflect a constriction of M_2 isograde due to extensional normal shearing prior to the M_3 metamorphism. Widespread normal shearing, however, is not observed between the phases D_2 and D_3. Accordingly, based on the present knowledge, this situation is inconsistent and needs further investigation.

6.3. METAMORPHISM M_3

SW-verging F_3 folding formed at the front of the north Himalayan nappe system and propagated towards SW (WYSS et al., 1999), affecting both the Tethyan Himalaya and the High Himalayan Crystalline. A common evolution of these two domains during D_3 is also reflected by M_3 metamorphic conditions that increase gradually from the NE to the SW from the lower chlorite zone in the Taktsi valley to the kyanite zone in the Tos valley (Plate 1). In the chlorite- and biotite zones, M_3 is a prograde metamorphism that is related to folding and subduction below the front of the North Himalayan Nappe System (WYSS et al., 1999). In the garnet- and kyanite zones, the M_2 mineral assemblage remained stable during M_3. Locally in these zones, a weakly developed M_3 mineral assemblage crystallized, containing similar minerals as the M_2 assemblage, indicating a continuous evolution from M_2 to M_3. As a consequence, in the High Himalayan Crystalline, F_3 folding occurred under conditions that were close to M_2 peak conditions without major cooling in the meantime and therefore, SW-verging F_3 folding affected the structures of the D_2 NE-verging Shikar Beh Nappe before exhumation started. According to EPARD et al. (1995), in the neighbouring Kullu valley area SW-verging folding was related to a slightly retrograde evolution compared with D_2.

6.4. METAMORPHISM M_4

During D_4 extrusion of the Crystalline Nappe the base of the High Himalayan Crystalline underwent a different M_4 metamorphic evolution than the central part (Figs 3 and 5, Plate 1). Related to SW-directed thrusting on D_4 shear bands in the Main Central Thrust Zone, the base of the High Himalayan Crystalline retrogressed from M_2/M_3 amphibolite facies conditions to greenschist facies conditions. The central part of the High Himalayan Crystalline by contrast underwent decompression under constant or slightly increasing temperatures within amphibolite facies conditions, coupled with NE-directed normal shearing and dextral strike-slip shearing within the Tos Dextral Transtension Zone. This is supported by rim P-T estimates indicating a pressure decrease from the SW to the NE in the High Himalayan Crystalline during M_4 (Fig. 10) and temperatures above T = 500 °C (Tab. 2).

6.5. THE TETHYAN HIMALAYA – HIGH HIMALAYAN CRYSTALLINE TRANSITION

D_4 Normal- and dextral strike-slip shearing is generally reported to be restricted to large-scale shear zones between the Tethyan Himalaya and the High Himalayan Crystalline. In these shear zones, the pre-D_4 isograde were constricted and therefore the low-grade metamorphic Tethyan Himalaya rocks appear to be juxtaposed directly against the high-grade metamorphic rocks of the High Himalayan Crystalline as reported, for example, from the Zanskar Shear Zone by DÈZES et al. (1999). On this basis, the Tethyan Himalaya and the High Himalayan Crystalline were considered as purely tectonic units. In the studied area by contrast, D_4 normal and dextral strike-slip shearing are distributed tectonostratigraphically over about 20 km, including the Tos- and Taktsi Dextral Transtension Zones. The geometrical arrangement of the shear zones as indicated in figure 1 suggests that the Taktsi Dextral Transtension Zone could be the equivalent of the Zanskar Shear Zone in the study area. Normal movement

in the Taktsi Dextral Transtension Zone, however, is characterized by fold reorientation, which accommodated only a relatively small shear displacement compared to normal shearing in the Zanskar Shear Zone. Consequently, the M_3 Barrovian-type metamorphic mineral zones remained undisturbed between the Tethyan Himalaya and the High Himalayan Crystalline, resulting in a gradual transition between these two domains. As a consequence, the Tethyan Himalaya and the High Himalayan Crystalline should be regarded as metamorphic zones rather than as tectonic units. It is proposed that the Tethyan Himalaya is restricted to the lower chlorite zone, whereas the biotite, garnet and kyanite zones make up the High Himalayan Crystalline. The upper chlorite zone represents the transition between these two domains. To compensate for a reduced shear displacement at the transition between the Tethyan Himalaya and the High Himalayan Crystalline, D_4 shearing shifted deep inside the High Himalayan Crystalline, where it formed the ductile Tos Dextral Transtension Zone.

6.6. INVERTED METAMORPHIC ZONATION

Two types of inverted metamorphic zonations occur in the High Himalayan Crystalline. The first type is a real inversion of metamorphic isograds by post-metamorphic deformation and the second one is the result of metamorphic overprint. The real inversion of metamorphic isograds is not recognizable in the field and was detected by thermobarometry. It is characterized by M_2 peak P-T conditions that decrease downsection within the kyanite zone, indicating an inversion of M_2 isotherms and isobars, a feature that cannot be explained by the geometry of the NE-directed D_2 Shikar Beh Nappe. It is suggested that the M_2 isograds were passively inverted during F_3 folding and/or during D_4 extrusion of the Crystalline Nappe, forming an open, SW-verging fold. A similar situation has already been encountered by EPARD et al. (1995) along the Mandi-Khoksar transect 50 km west of the studied section. On the basis of model calculations assuming a pre-Main Central Thrust metamorphism (M_2 in this study) and varying thermal conductivities of the Tethyan Himalaya, the High Himalayan Crystalline and the Lesser Himalayan Sequence during thrusting in the neighbouring Kullu valley area, GRASEMANN (1993) proposed that inversion of isotherms may be possible in the overthrust Crystalline Nappe due to thrusting along the Main Central Thrust. These inverted isotherms are considered to be the result of a pre-thrust metamorphism (M_2 in this study) and a syn-thrust metamorphism (M_3 and/or M_4 in this study) during a continuous metamorphic evolution. Applied to the studied area, GRASEMANN'S (1993) model suggests that the downsection decrease in peak metamorphic conditions within the Crystalline Nappe is the result of an inversion of M_3 and/or M_4 isotherms during D_3/D_4 due to previous M_2 thermal disturbances. This contrasts with the results presented in this study that indicate a passive deformation of M_2 isotherms during D_3/D_4. Consequently, as it lays emphasis on the syn-Main Central Thrust metamorphic crystallization for the formation of inverted isotherms and as it assumes that the pre-Main Central Thrust metamorphism M_2 is of subordinate importance in the High Himalayan Crystalline, GRASEMANN'S (1993) model cannot be adapted to the studied traverse.

The second type of zonation is a combination of M_4 greenschist facies and sillimanite zone metamorphic overprint of the M_2/M_3 kyanite zone mineral assemblage in the D_4 Main Central Thrust Zone and in the Tos Dextral Transtension Zone, respectively. D_4 thrusting along the Main Central Thrust Zone occurred under M_4 greenschist facies conditions that were prograde in the underlying Lesser Himalayan Sequence and retrograde at the base of the Crystalline Nappe, where a mineral assemblage containing mainly chlorite, biotite and muscovite overprinted the M_2/M_3 kyanite zone assemblage. This gives the impression of an increase upsection in metamorphic conditions from M_4 greenschist facies rocks in the Lesser Himalayan Sequence and at the base of the Crystalline Nappe to overlying M_2/M_3 kyanite zone rocks (Plate 1). Retrogression at the base of the Crystalline Nappe may be explained as an effect of cooling by heat flow into the cold overridden Lesser Himalayan Sequence, that was simultaneously heated up by the hot overriding Crystalline Nappe, according to the model proposed by LE FORT (1975). Changing metamorphic conditions due to decompression during D_4 transtension in the Tos Dextral Transtension Zone lead to an overprint of the M_2/M_3 kyanite-bearing mineral assemblage by M_4 sillimanite in D_4 shear zones, giving the impression of metamorphic conditions increasing upsection from the M_2/M_3 kyanite zone to the M_4 sillimanite zone (Plate 1). As the increase in metamorphic conditions upsection, from M_4 greenschist facies conditions in the Main Central Thrust Zone over M_2/M_3 kyanite zone conditions to M_4 sillimanite zone conditions in the Tos Dextral Transtension Zone is the result of a polymetamorphic evolution, it has to be referred to as an apparent inverted metamorphic zonation.

7. Conclusions

Along the traverse from the Spiti valley through eastern Lahul to the Parvati valley, four stages of metamorphic crystallization M_1 to M_4 are distinguished, related to the four deformational phases D_1 to D_4. M_1 represents an independent metamorphic cycle that first reached kyanite and then sillimanite zone peak conditions in the High Himalayan Crystalline, indicating considerable crustal thickening, that is either of pre- or of early Himalayan age.

M_2 is the main Tertiary metamorphism in the High Himalayan Crystalline, related to the NE-verging D_2 stacking of the Shikar Beh Nappe. M_2 peak conditions increase from the top of the High Himalayan Crystalline downsection from $T \approx 520$ °C and $P \approx 500$ MPa to $T \approx 700$ °C and $P \approx 850$ MPa in the center of the High Himalayan Crystalline. From there on, M_2 conditions decrease downsection towards the base of the High Himalayan Crystalline to $T \approx 650$ °C and $P \approx 720$ MPa. This inversion of M_2 isotherms and isobars is suggested to result from passive folding of M_2 isograds during D_3 and/or D_4, representing a real inverted metamorphic zonation.

M_3 is the main metamorphism in the Tethyan Himalaya, related to the SW-verging F_3 folding. In the High Himalayan Crystalline by contrast, M_3 represents the continuation of M_2 conditions and involved only minor mineral growth. M_3 metamorphic conditions increase gradually from the Tethyan Himalaya to the underlying High Himalayan Crystalline, indicating that these domains represent metamorphic zones rather than tectonic units in the studied area.

During D_4 extrusion of the Crystalline Nappe, M_4 conditions were related to different structures and reached different metamorphic conditions at the base and in the center of the High Himalayan Crystalline. At the base of the High Himalayan Crystalline M_4 is characterized by retrograde greenschist facies conditions related to SW-verging thrusting along the Main Central Thrust, that overprinted the M_2/M_3 kyanite zone mineral assemblage. Retrogression to greenschist facies conditions is interpreted as the result of cooling by heat flow into the cooler, overridden Lesser Himalayan Sequence, that simultaneously underwent prograde greenschist facies metamorphism. In a higher crustal level M_4 reached sillimanite zone conditions related to D_4 normal- and dextral strike-slip movement, overprinting the M_2/M_3 kyanite zone mineral assemblage in the Tos Dextral Transtension Zone. D_4 is associated with decompression that increases upsection from the base of the High Himalayan Crystalline to its center.

The M_4 overprint on the M_2/M_3 mineral assemblage leads to an increase in metamorphic conditions upsection from M_4 greenschist facies conditions over M_2/M_3 kyanite zone conditions to M_4 sillimanite zone conditions in the High Himalayan Crystalline. This increase is the result of a polymetamorphic evolution and has therefore to be referred to as an apparent inverted metamorphic zonation.

This study demonstrates that a real and an apparent inverted metamorphic zonation occur within the same section in a relatively small area compared to the whole Himalayan chain. As a consequence, for further studies about this phenomenon, it will be important to distinguish between inverted metamorphic field gradients assigned to one stage of metamorphic crystallisation only and apparent inverted metamorphic zonations resulting from metamorphic overprint due to a polyphase metamorphic evolution. Given the significant geological variations observed all along the Himalayan orogen, it is expected that several models must be allowed to coexist to explain the different features integrated into what is referred to as the inverted metamorphic zonation.

Acknowledgements

This study was financed by the University of Lausanne and the Swiss National Science Foundation (FNRS grant 20-38917.93, project: Albrecht Steck, University of Lausanne). I am grateful to Georges Mascle, who helped to organize the transport of samples, to François Bussy for support and discussion during microprobe analysis and to Jean-Claude Lavanchy for XRF determinations. Linguistic revision and critical comments of Albrecht Steck and Neil Mancktelow are greatfully acknowledged. The manuscript benefited from reviews by Georg Hoinkes and Martin Frey. Last but not least, I wish to thank Raymond Ansermoz and Laurent Nicod for preparation of innumerable thin sections.

References

ARGLES, T.W., PRINCE, C.I., FOSTER, G.L. and VANCE, D. (1999): New garnets for old? Cautionary tales from young mountain belts. Earth Planet. Sci. Lett. 172, 301–309.

BASSOULET, J. P., COLCHEN, M., JUTEAU, T., MARCOUX, J. and MASCLE, G. (1980): L'édifice des nappes du Zanskar (Ladakh-Himalaya). C. R. Acad. Sc. Paris 290D, 389–392.

BESSE, J., COURTILLOD, V., POZZI, J.P. and ZHOU, Y.X. (1984): Paleomagnetic estimates of Cenozoic convergence in the Himalayan Thrusts and Tsangbo suture. Nature 311, 621–626.

BHAT, M.I. and LE FORT, P. (1992): Sm–Nd age and petrogenesis of Rampur metavolcanic rocks, NW Himalayas: Late Archean relics in the Himalayan belt. Precambrian Res. 56, 191–210.

BRUN, J.P., BURG, J.P. and MING, C.G. (1985): Strain trajectories above the Main Central Thrust (Himalaya) in southern Tibet. Nature 313, 388–390.

BRUNEL, M. and KIENAST, J.-R. (1986): Etude pétrostructurale des chevauchements ductiles himalayens sue la transversale de l'Everest-Makalu (Népal oriental). Canad. J. Earth Sci. 23, 1117–1137.

BURCHFIEL, B.C. and ROYDEN, L.H. (1985): North-south extension within the convergent Himalayan region. Geology 13, 679–682.

BURCHFIEL, B.C., ZHILIANG, C., HODGES, K.V., YUPING, L., ROYDEN, L.H., CHANGRONG, D. and JIENE, X. (1992): The South Tibetan Detachment System, Himalayan Orogen: Extension contemporaneous with and parallel to shortening in a collisional mountain belt. Spec. Pap. Geol. Soc. Am. 269, 1–41.

BURG, J.P., BRUNEL, M,. GAPAIS, D., CHEN, G.N. and LIU, G.H. (1984): Deformation of leucogranites of the crystalline Main Central Sheet in southern Tibet (China). J. Struct. Geol. 6, 535–542.

DAVIDSON, C., GRUJIC, D.E., HOLLISTER, L.S. and SCHMID, S.M. (1997): Metamorphic reactions related to decompression and synkinematic intrusion of leucogranite, High Himalayan Crystallines, Bhutan. J. Metamorphic Geol. 15, 593–612.

DÈZES, P., VANNAY, J.C., STECK, A., BUSSY, F. and COSCA, M. (1999): Synorogenic extension; quantitative constraints on the age and displacement of the Zanskar Shear Zone (NW Himalaya). Geol. Soc. Am. Bull. 111/3, 364–374.

EPARD, J.L., STECK, A., VANNAY, J.C. and HUNZIKER, J. (1995): Tertiary Himalayan structures and metamorphism in the Kulu Valley (Mandi-Khoksar transect of the Western Himalaya) – Shikar Beh Nappe and Crystalline Nappe. Schweiz. Mineral. Petrogr. Mitt. 75, 59–84.

FERRARA, G., LOMBARDO, B. and TONARINI, S. (1983): Rb/Sr Geochronology of Granites and Gneisses from the Mount Everest Region, Nepal Himalaya. Geol. Rundsch. 72, 119–136.

FRANK, W., HOINKES, G., MILLER, C., PURTSCHELLER, F., RICHTER, W. and THÖNI, M. (1973): Relations between Metamorphism and Orogeny in a Typical Section of the Indian Himalayas. Tscherm. Min. Petr. Mitt. 20, 303–332.

FRANK, W., THÖNI, M. and PURTSCHELLER, F. (1977): Geology and petrography of Kulu-South Lahul area. Colloq. int. C.N.R.S. 268/2, 147–172.

FRANK, W., GRASEMANN, B., GUNTLI, P. and MILLER, C. (1995): Geological Map of the Kishtwar – Chamba-Kulu Region (NW Himalayas, India). Jb. Geol. B.-A. Wien 138/2, 299–308.

FUCHS, G. (1987): The Geology of southern Zanskar (Ladakh) – Evidence for the autochthony of the Tethys Zone of the Himalaya. Jb. Geol. B.-A. Wien 130/4, 465–491.

FUCHS, G. (1992): Pre-Alpine and Alpine Orogenic Phases in the Himalaya. In: SINHA, A.K. (ed.): Himalayan Orogen and Global Tectonics. The International Lithosphere Programme Publ. 197, A.A. Balkema Rotterdam, 19–34.

GAETANI, M. and GARZANTI, E. (1991): Multicyclic History of the Northern India Continental margin (Northwestern India). Bull. Amer. Assoc. Petroleum Geol. 75 (9), 1427–1446.

GANSSER, A. (1964): Geology of the Himalayas. John Wiley & Sons, London, 289pp.

GAPAIS, D., PÊCHER, A., GILBERT, E. and BALLÈVRE, M. (1992): Synconvergence spreading of the higher Himalaya crystalline in Ladakh. Tectonics 11, 1045–1056.

GARZANTI, E., CASNEDI, R. and JADOUL, F. (1986): Sedimentary evidence of a Cambro-Ordovician orogenic event in the Northwestern Himalaya. Sed. Geol. 48, 237–265.

GARZANTI, E., BAUD, E. and MASCLE, G. (1987): Sedimentary record of the northward flight of India and its collision with Eurasia (Ladakh Himalaya, India). Geodin. Acta 1, 297–312.

GARZANTI, E., CRITELLI, S. and INGERSOLL, R.V. (1996): Paleogeographic and paleotectonic evolution of the Himalayan Range as reflected by detrital modes of Tertiary sandstones and modern sands (Indus transect, India and Pakistan). Geol. Soc. Am. Bull. 108/6, 631–642.

GRASEMANN, B. (1993): Numerical modeling of the thermal history of the Himalayas, Kullu valley, India. In: TRELOAR, P.J. and SEARLE, M.P. (eds): Himalayan Tectonics. Geol. Soc. Spec. Publ. London 74, 237–249.

GROVE, T.L., BAKER, M.B. and KINZLER, R.J. (1984): Coupled CaAl-NaSi diffusion in plagioclase feldspar: Experiments and applications to cooling rate speedometry. Geochim. Cosmochim. Acta 48, 2113–2121.

GRUJIC, D., CASEY, M., DAVIDSON, C., HOLLISTER, L.S., KÜNDIG, R., PAVLIS, T. and SCHMID, S. (1996): Ductile extrusion of the Higher Himalayan Crystalline in Bhutan: evidence from quartz microfabrics. Tectonophysics 260, 21–43.

GUNTLI, P. (1993): Geologie und Tektonik des Higher und Lesser Himalaya im Gebiet von Kishtwar, SE-Kashmir (NW Indien). Ph.D thesis nr. 10211, ETH Zürich, 198pp.

HAYDEN, H.H. (1904): The Geology of Spiti, with parts of Bashar and Rupshu. Mem. Geol. Surv. India 36, 1–129.

HERREN, E. (1987): Northeast-southwest extension within the Higher Himalayas (Ladakh, India). Geology 15, 409–413.

HODGES, K.V. and SPEAR, F.S. (1982): Geothermometry, geobarometry and the Al_2SiO_5 triple point at Mt. Moosilauke, New Hampshire. Am. Mineral. 67, 1118–1134.

HODGES, K.V. and CROWLEY, P.D. (1985): Error estimation and empirical geothermobarometry for pelitic systems. Am. Mineral. 70, 702–709.

HUBBARD, M.S. (1996): Ductile shear as a cause of Inverted Metamorphism: Example from the Napal Himalaya. J. Geol. 104, 493–499.

HUBBARD, M.S. (1989): Thermobarometric constraints on the thermal history of the Main Central Thrust Zone and the Tibetan Slab, eastern Nepal Himalaya. J. Metamorphic Geol. 7, 19–30.

JAIN, A.K., GOEL, R.K. and NAIR, N.G.K. (1980): Implications of pre-mesozoic orogeny in the geological evolution of the Himalaya and Indo-Gangetic plains. Tectonophysics 62, 67–86.

JAIN, A.K. and MANICKAVASAGAM, R.M. (1993): Inverted metamorphism in the intracontinental ductile shear zone during Himalayan collision tectonics. Geology 21, 407–410.

JAMIESON, R.A., BEAUMONT, C., HAMILTON, J.K. and FULLSACK, P. (1996): Tectonic assembly of inverted metamorphic sequences. Geology 24/9, 839–842.

LE FORT, P. (1975): Himalayas: The collided Range. Present knowledge of the continental arc. Am. J. Sci. 175-A, 1–44.

LE BRETON, N. and THOMPSON, A.B. (1988): Fluid-absent (dehydration) melting of biotite in metapelites in the early stages of crustal anatexis. Contr. Mineral. Petrol. 99, 226–237.

MALLET, F.R. (1875): On the geology and mineral ressources of the Darjiling district and the western Duars. Mem. Geol. Surv. India 11, 1–50.

METCALFE, R.P. (1993): Pressure, temperature and time constraints on metamorphism across the Main Central Thrust Zone and the High Himalayan Slab in the Garhwal Himalaya. In: TRELOAR, P.J. and SEARLE, M. P. (eds): Himalayan Tectonics. Geol. Soc. Spec. Publ. London 74, 485–509.

NISBET, E.G., DIETRICH, V.J. and EISENWEIN, A. (1979): Routine trace element determination in silicate minerals and rocks by X-ray fluorescence. Fortschr. Mineral. 57, 264–279.

PANDE, I.C. and SAXENA, M.N. (1968): Birth and development of the Himalayas, Publ. Centre Adv. Study Geol., Punjab Univ. 4, Chandigarh.

PATRIAT, P. and ACHACHE, J. (1984): India-Eurasia collision chronology has implications for crustal shortening and driving mechanism of plates. Nature 311, 615–621.

PÊCHER, A. (1991): The contact between the Higher Himalaya Crystallines and the Tibetan sedimentary series: Miocene large-scale dextral shearing. Tectonics 10, 587–598.

PÊCHER, A. and SCAILLET, B. (1989): La structure du Haut-Himalaya au Gharwal (Indes). Eclogae geol. Helv. 82, 655–668.

PÊCHER, A., BOUCHEZ, I.L., and LE FORT, P. (1991): Miocene dextral shearing between Himalaya and Tibet. Geology 19, 683–685.

POGNANTE, U. and LOMBARDO, B. (1989): Metamorphic evolution of the High Himalayan Crystallines in SE Zanskar, India. J. Metamorphic Geol. 7, 9–17.

SAXENA, M.N. (1973): Problems in Himalayan geology. Geol. Rundsch. 162, 563–581.

SAXENA, M.N. (1980): Orogenic and epeirogenic cycles in the Himalaya. Himalayan Geology 10, 191–210.

SEARLE, M.P. (1986): Structural evolution and sequence of thrusting in the High Himalayan, Tibetan-Tethys and Indus suture zones of Zanskar and Ladakh, Western Himalaya. J. Struct. Geol. 8, 923–936.

SEARLE, M.P., COOPER, D.J.W. and REX, A.J. (1988): Collision tectonics of the Ladakh-Zanskar Himalaya. Philos. Trans. R. Soc. London A 326, 117–150.

SEARLE, M.P. and REX, A.J. (1989): Thermal model for the Zanskar Himalaya. J. Metamorphic Geol. 7, 127–134.

SEARLE, M.P., WATERS, D.J., REX, D.C. and WILSON, R.N. (1992): Pressure, temperature and time constraints on Himalayan metamorphism from eastern Kashmir and western Zanskar. J. Geol. Soc. London 149, 753–773.

SPEAR, F.S. (1991): On the interpretation of peak metamorphic temperatures in the light of garnet diffusion during cooling. J. Metamorphic Geol. 9, 379–388.

SPEAR, F.S. (1993): Metamorphic Phase Equilibria and Pressure-Temperature-Time Paths. Min. Soc. Am. Monograph, Washington D.C.

SPEAR, F.S. and CHENEY, J.T. (1989): A petrogenetic grid for pelitic schists in the system SiO_2–Al_2O_3–FeO–MgO–K_2O–H_2O. Contrib. Mineral. Petrol. 101, 149–164.

SPEAR, F.S. and FLORENCE, F.P. (1992): Thermobarometry in granulites: Pitfalls and new approaches. J. Precambrian Res. 55, 209–241.

SPRING, L. (1993): Structures gondwaniennes et himalayaennes dans la zone tibétaine du Haut Lahul-Zanskar oriental (Himalaya Indien). Mém. Géol. Lausanne 14, 148pp.

STECK, A., SPRING, L., VANNAY, J.C., MASSON, H., BUCHER, H., STUTZ, E., MARCHANT, R. and TIÈCHE, J.C. (1993): Geological transect across the northwestern Himalaya in eastern Ladakh and Lahul (a model for the continental collision of India and Asia). Eclogae geol. Helv. 86, 219–263.

STECK, A., EPARD, J.L., VANNAY, J.C., HUNZIKER, J., GIRARD, M., MORARD, A. and ROBYR, M. (1998): Geological transect across the Tso Morari and Spiti areas – The nappe structures of the Tethys Himalaya. Eclogae geol. Helv. 91, 103–121.

STECK, A., EPARD, J.L. and ROBYR, M. (1999): The NE-directed Shikar Beh Nappe: A major structure of the Higher Himalaya. Eclogae geol. Helv. 92, 239–250.

SWAPP, S.M. and HOLLISTER, L.S. (1991): Inverted metamorphism within the Tibetan Slab of Bhutan: evidence for a tectonically transported heat source. Canad. Mineral. 29, 1019–1041.

THOMPSON, A.B. and TRACY, R.J. (1979): Model systems for anatexis of pelitic rocks: facies series melting and reactions in the system CaO–$KAlO_2$–$NaAlO_2$–Al_2O_3–SiO_2–H_2O. Contrib. Mineral. Petrol. 70, 429–238.

THÖNI, M. (1977): Geology, Structural Evolution and Metamorphic Zoning in the Kulu Valley (Himachal Himalayas, India) with special reference to the Reversed Metamorphism. Mitt. Ges. Geol. Bergbaustud. Österr. 24, 125–187.

TRELOAR, P.J., BROUGHTON, R.D., WILLIAMS, M.P., COWARD, M.P. and WINDLEY, B.F. (1989): Deformation, metamorphism and imbrication of the Indian plate, south of the Main Mantle Thrust, north Pakistan. J. Metamorphic Geol. 7, 111–125.

VANNAY, J.C. (1993): Géologie des chaînes du Haut-Himalaya et du Pir Panjal au Haut-Lahul (NW Himalaya, Inde): Paléogéographie et tectonique. Mém. Géol. Lausanne 16, 148pp.

VANNAY, J.C. and STECK, A. (1995): Tectonic evolution of the High Himalaya in Upper Lahul (NW Himalaya, India). Tectonics 14, 253–263.

VANNAY, J.C. and GRASEMANN, B. (1998): Inverted metamorphism in the High Himalaya of Himachal Pradesh (NW India): Phase equilibria versus thermobarometry. Schweiz. Mineral. Petrogr. Mitt. 78, 107–132.

VALDIYA, K.S. (1995): Proterozoic sedimentation and Pan-African geodynamic development in the Himalaya. Precambrian Res. 74, 35–55.

WALKER, J.D., MARTIN, M.W., BOWRING, S.A. SEARLE, M.P., WATERS, D.J. and HODGES, K.V. (1999): Metamorphism, Melting and Extension: Age constraints from the High Himalayan Slab of Southeast Zanskar and Northwest Lahul. J. Geol. 107, 473–495.

WYSS, M., HERMANN, J. and STECK, A. (1999): Structural and metamorphic evolution of the northern Himachal Himalaya, NW India (Spiti–eastern Lahul-Parvati valley traverse). Eclogae geol. Helv. 92, 3–44.

WYSS, M. and HERMANN, J. (submitted): Himalayan olivine gabbros: Evidence for extension-related magmatism and early granulite facies metamorphism. Tectonics.

Manuscript received August 17, 1999: revision accepted September 2, 2000.

Appendix

THERMOBAROMETRY

In the garnet and kyanite zones of the studied section 36 samples containing relevant mineral phases were chosen for thermobarometry. On these samples a two-step analytical procedure was applied.

Step 1: To characterize the compositional zoning in garnet a rough garnet composition traverse was measured in all samples chosen for thermobarometry (Figs 8, A1). On the basis of these traverses 11 samples were chosen that meet to the following requirements: (1) they are representative for the garnet and kyanite zone assemblages and (2) their traverses show a compositional zoning.

Step 2: To estimate the apparent peak temperatures the zone of Fe/(Fe + Mg) minimum was determined for each garnet on the basis of the compositional traverse established in step 1 and for each garnet a series of 10 to 20 additional radial compositional traverses across this zone towards the rim was measured (Fig. A1). These traverses comprise the compositions at the Fe/(Fe + Mg) minima and the rim compositions, each of them contains 20 to 40 analyses.

Compositional traverses across plagioclase, biotite and muscovite were also measured. With the exception of plagioclase from the garnet zone, these minerals do not show considerable variations from core to rim. An average of 60 analyses were performed for each of these mineral phases per sample.

Mineral compositions were measured using a Cameca SX50 electron microprobe. The acceleration voltage was 15 kV for all phases and the nominal beam current was 25 nA for garnet, 15 nA for biotite and muscovite, and 10 nA for plagioclase.

Representative garnet compositions at the Fe/(Fe + Mg) minimum, garnet rim compositions and plagioclase, biotite and muscovite compositions are presented in tables A1 to A4. Pressures and temperatures were calculated with a computer program written by Frank S. Spear (GTB 68), using the thermobarometers and calibrations listed in table 1.

BULK ROCK ANALYSES

The bulk chemical compositions were determined by X-ray fluorescence (XRF) analyses with a sequential spectrometer using natural USGS rock samples for calibration. Rocks were ground in a tungsten carbide mill. Major elements were determined using glass beads which were fused from ignited rocks powders (at 1050 °C) mixed with $Li_2B_4O_7$ in a 1/5 ratio in gold platinum pans at 1150 °C. The intensities were corrected for instrumental drift, background and matrix effects. The trace elements were determined by XRF analyses of 10g rock powder samples using the synthetic background method for which major elements have to be known (NISBET et al., 1979).

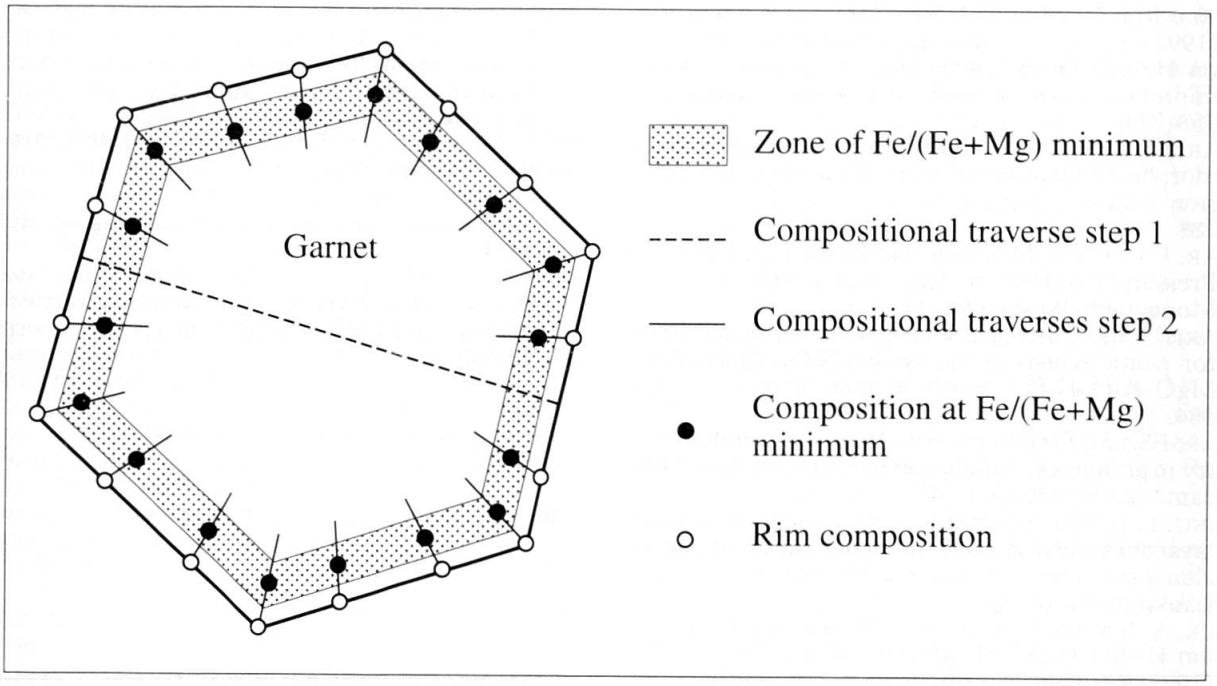

Fig. A1 Two-step analytical procedure for garnet compositional traverses.

Tab. A1 Representative garnet compositions

Garnet compositions at Fe/(Fe + Mg) minima								
Sample	EMP 2	EMP 3	EMP 4	EMP 6	EMP 7	EMP 8	EMP 10	EMP 11
SiO_2	36.64	36.60	37.45	37.58	37.05	37.35	37.18	37.38
TiO_2	0.02	0.01	0.03	0.03	0.01	0.03	0.00	0.02
Al_2O_3	20.43	20.23	20.96	20.89	20.55	20.78	20.85	20.75
Cr_2O_3	0.05	0.09	0.04	0.04	0.04	0.05	0.04	0.05
FeO	32.50	33.19	34.13	34.05	35.53	33.81	34.65	34.36
MnO	4.00	4.23	2.26	1.20	1.84	2.23	0.74	0.53
MgO	3.48	3.30	4.17	4.40	3.36	4.15	4.59	4.63
CaO	2.37	1.99	1.97	2.89	1.96	2.28	2.06	2.40
Total	99.52	99.64	101.02	101.05	100.33	100.67	100.12	100.19
Cations normalized to 12 oxygens								
Si	2.97	2.98	2.98	2.98	2.99	2.98	2.98	2.98
Ti	0.00	0.00	0.00	0.00	0.00	0.00	0.00	0.00
Al	1.95	1.94	1.97	1.95	1.95	1.96	1.97	1.96
Cr	0.00	0.00	0.00	0.00	0.00	0.00	0.00	0.00
Fe_{tot}	2.20	2.26	2.27	2.26	2.39	2.25	2.32	2.29
Mn	0.27	0.29	0.15	0.08	0.12	0.15	0.06	0.03
Mg	0.42	0.40	0.49	0.52	0.40	0.49	0.55	0.56
Ca	0.20	0.17	0.17	0.24	0.17	0.19	0.18	0.20
Sum	8.04	8.05	8.04	8.04	8.04	8.04	8.04	8.03
X_{Fe}	0.70	0.72	0.74	0.72	0.77	0.72	0.75	0.74
X_{Mg}	0.13	0.13	0.16	0.16	0.13	0.16	0.18	0.17
X_{Mn}	0.08	0.09	0.05	0.02	0.04	0.05	0.01	0.02
X_{Ca}	0.06	0.06	0.06	0.08	0.06	0.63	0.06	0.07
Fe/(Fe+Mg)	0.84	0.85	0.82	0.81	0.86	0.82	0.80	0.81

Garnet rim compositions									
Sample	EMP 1	EMP 2	EMP 3	EMP 4	EMP 6	EMP 7	EMP 8	EMP 10	EMP 11
SiO_2	36.46	35.96	36.35	36.86	37.17	37.05	36.97	37.15	36.83
TiO_2	0.01	0.02	0.03	0.02	0.03	0.00	0.02	0.01	0.04
Al_2O_3	20.35	20.23	20.32	20.78	20.56	20.56	20.54	20.58	20.53
Cr_2O_3	0.03	0.06	0.03	0.07	0.06	0.04	0.06	0.02	0.04
FeO	29.26	32.06	31.84	23.92	33.61	36.20	34.56	35.63	35.94
MnO	8.15	7.17	7.30	5.33	3.27	1.99	3.56	0.91	0.98
MgO	1.67	2.21	2.10	3.10	3.04	2.54	2.62	3.38	3.29
CaO	3.66	1.35	1.24	1.43	2.88	2.04	1.93	2.52	2.32
Total	99.36	99.09	99.22	100.51	100.65	99.93	100.29	100.23	99.97
Cations normalized to 12 oxygens									
Si	2.98	2.96	2.99	2.97	2.99	2.97	2.99	2.99	2.98
Ti	0.00	0.00	0.00	0.00	0.00	0.00	0.00	0.00	0.99
Al	1.96	1.96	1.97	1.98	1.96	1.97	1.96	1.95	1.96
Cr	0.00	0.00	0.00	0.00	0.00	0.00	0.00	0.00	0.00
Fe_{tot}	2.00	2.21	2.19	2.22	2.26	2.46	2.34	2.40	2.43
Mn	0.56	0.50	0.50	0.37	0.22	0.13	0.24	0.06	0.07
Mg	0.20	0.27	0.26	0.37	0.37	0.30	0.31	0.40	0.34
Ca	0.32	0.12	0.10	0.12	0.25	0.18	0.16	0.22	0.20
Sum	8.03	8.04	8.02	8.03	8.04	8.04	8.02	8.03	8.04
X_{Fe}	0.64	0.72	0.71	0.72	0.73	0.81	0.76	0.77	0.79
X_{Mg}	0.06	0.08	0.09	0.12	0.12	0.10	0.10	0.13	0.12
X_{Mn}	0.18	0.16	0.16	0.11	0.07	0.04	0.08	0.02	0.02
X_{Ca}	0.10	0.03	0.04	0.04	0.08	0.06	0.06	0.07	0.06
Fe/(Fe+Mg)	0.90	0.89	0.88	0.85	0.86	0.88	0.88	0.86	0.87

Tab. A2 Representative plagioclase compositions.

Plagioclase rim compositions									
Sample	EMP 1	EMP 2	EMP 3	EMP 4	EMP 6	EMP 7	EMP 8	EMP 10	EMP 11
SiO_2	61.01	62.97	63.22	63.12	62.61	61.56	60.20	62.90	62.56
Al_2O_3	23.82	23.48	22.83	23.66	23.73	24.37	24.45	23.47	23.45
FeO	0.19	0.18	0.07	0.18	0.15	0.04	0.08	0.08	0.05
MgO	0.00	0.00	0.00	0.00	0.00	0.00	0.00	0.00	0.00
CaO	5.48	4.68	4.02	4.94	5.08	5.83	5.84	4.91	4.89
Na_2O_3	8.56	9.03	9.37	8.87	8.78	8.26	8.32	8.96	8.94
K_2O	0.12	0.07	0.17	0.09	0.11	0.14	0.11	0.05	0.06
Total	99.19	100.44	99.69	100.86	100.50	100.20	99.04	100.36	99.96
Cations normalized to 8 oxygens									
Si	2.73	2.77	2.80	2.77	2.76	2.72	2.70	2.78	0.77
Al	1.26	1.22	1.19	1.22	1.23	1.27	1.23	1.22	1.23
Fetot	0.00	0.00	0.00	0.00	0.00	0.00	0.00	0.00	0.00
Mg	0.00	0.00	0.00	0.00	0.00	0.00	0.00	0.00	0.00
Ca	0.26	0.22	0.19	0.23	0.24	0.28	0.28	0.23	0.23
Na	0.74	0.77	0.80	0.76	0.75	0.71	0.72	0.76	0.77
K	0.01	0.00	0.01	0.01	0.01	0.01	0.01	0.00	0.00
Sum	5.01	5.00	5.00	4.99	5.00	4.99	5.01	4.99	5.00
X_{ab}	0.73	0.77	0.80	0.76	0.75	0.71	0.71	0.77	0.77
X_{an}	0.26	0.22	0.19	0.23	0.24	0.28	0.28	0.23	0.23
X_{or}	0.01	0.01	0.01	0.01	0.01	0.01	0.01	0.00	0.00

Tab. A3 Representative biotite compositions.

Biotite rim compositions									
Sample	EMP 1	EMP 2	EMP 3	EMP 4	EMP 6	EMP 7	EMP 8	EMP 10	EMP 11
SiO_2	35.71	35.22	35.16	36.32	35.46	35.42	35.36	36.23	35.96
TiO_2	1.81	1.93	2.70	2.38	2.46	2.72	2.44	1.70	1.72
Al_2O_3	18.82	18.77	18.85	19.38	19.11	18.50	18.62	18.66	18.92
FeO	19.87	19.89	20.14	18.13	20.07	20.34	19.39	16.77	17.08
MnO	0.20	0.18	0.19	0.15	0.15	0.04	0.10	0.08	0.04
MgO	9.50	10.03	8.86	10.39	9.12	9.34	10.00	12.12	11.76
CaO	0.00	0.00	0.00	0.00	0.00	0.00	0.00	0.00	0.00
Na_2O	0.10	0.30	0.23	0.32	0.20	0.25	0.20	0.31	0.32
K_2O	9.54	9.17	9.19	9.11	9.16	9.14	8.78	8.86	8.67
F	0.00	0.00	0.00	0.00	0.00	0.00	0.00	0.00	0.00
Total	95.57	95.49	95.33	96.18	95.75	95.77	94.91	94.98	94.85
Cations normalized to 11 oxygens									
Si	2.71	2.68	2.68	2.71	2.69	2.69	2.69	2.72	2.71
Ti	0.10	0.11	0.15	0.13	0.14	0.16	0.14	0.09	1.00
Al	1.69	1.69	1.69	1.7	1.70	1.66	1.67	1.66	1.68
Fe_{tot}	1.27	1.27	1.28	1.13	1.27	1.29	1.24	1.06	1.08
Mn	0.01	0.01	0.01	0.01	0.01	0.00	0.01	0.01	0.00
Mg	1.07	1.14	1.00	1.15	1.03	1.06	1.14	1.36	1.32
Ca	0.00	0.00	0.00	0.00	0.00	0.00	0.00	0.00	0.00
Na	0.01	0.04	0.04	0.05	0.03	0.04	0.31	0.04	0.05
K	0.92	0.89	0.90	0.86	0.89	0.89	0.85	0.85	0.83
F	0.00	0.00	0.00	0.00	0.00	0.00	0.00	0.00	0.00
Sum	7.80	7.83	7.77	7.76	7.77	7.78	7.77	7.80	7.79
X_{ann}	0.44	0.43	0.45	0.39	0.44	0.45	0.42	0.36	0.37
X_{phl}	0.37	0.39	0.35	0.40	0.36	0.37	0.39	0.45	0.46

Tab. A4 Representative muscovite compositions.

Muscovite rim compositions									
Sample	EMP 1	EMP 2	EMP 3	EMP 4	EMP 6	EMP 7	EMP 8	EMP 10	EMP 11
SiO_2	46.16	45.86	45.71	45.89	46.01	46.07	45.97	45.98	46.16
TiO_2	0.48	0.77	0.77	0.91	0.89	0.94	0.86	0.67	0.81
Al_2O_3	34.75	34.92	34.48	35.40	35.24	34.86	35.13	35.30	34.97
FeO	1.64	1.94	2.11	1.15	1.27	1.43	1.31	1.16	1.13
MnO	0.05	0.02	0.03	0.02	0.02	0.03	0.02	0.00	0.02
MgO	0.91	0.72	0.74	0.75	0.73	0.81	0.83	0.79	0.93
CaO	0.01	0.00	0.01	0.01	0.00	0.00	0.00	0.00	0.02
Na_2O	0.90	1.27	1.09	1.10	0.87	0.98	0.96	1.67	1.58
K_2O	10.17	9.68	9.86	9.91	10.15	10.09	10.06	9.05	9.09
F	0.00	0.00	0.00	0.00	0.00	0.00	0.00	0.00	0.00
Total	95.08	95.17	94.80	95.15	95.18	95.19	95.15	94.69	94.71
Cations normalized to 11 oxygens									
Si	3.08	3.06	3.07	3.06	3.07	3.07	3.06	3.06	3.07
Ti	0.02	0.04	0.04	0.05	0.04	0.05	0.04	0.03	0.04
Al	2.73	2.75	2.73	2.78	2.77	2.74	2.76	2.77	2.75
Fe_{tot}	0.09	0.11	0.12	0.06	0.07	0.08	0.07	0.07	0.06
Mn	0.00	0.00	0.00	0.00	0.00	0.00	0.00	0.00	0.00
Mg	0.09	0.72	0.07	0.74	0.07	0.08	0.08	0.08	0.09
Ca	0.00	0.00	0.00	0.00	0.00	0.00	0.00	0.00	0.00
Na	0.12	0.16	0.14	0.14	0.11	0.13	0.13	0.22	0.20
K	0.87	0.83	0.85	0.84	0.86	0.86	0.86	0.77	0.77
F	0.00	0.00	0.00	0.00	0.00	0.00	0.00	0.00	0.00
Sum	7.01	7.02	7.02	7.00	6.99	7.00	7.00	7.00	6.99
X_{ms}	0.88	0.83	0.86	0.86	0.85	0.87	0.87	0.78	0.79
X_{pg}	0.12	0.17	0.14	0.14	0.15	0.13	0.13	0.22	0.21

Plate 1 Sections for the Spiti valley-eastern Lahul-Parvati valley area showing metamorphic mineral zones for pelitic rocks. Tracks of the sections I and II are indicated in figure 1 (inset B), simplified after WYSS et al. (1999). For each mineral zone, the mineral assemblages corresponding to the stages of metamorphic crystallization M_1 to M_4, the index mineral, schistosities S_x and deformational phases D_x are indicated. In the kyanite zone, the occurrence of sillimanite in the Tos Dextral Transtension Zone is indicated. Note that the transition from the Tethyan Himalaya into the High Himalayan Crystalline is gradual and note the abrupt decrease of M_2 metamorphic conditions between the garnet zone and the biotite zone. For abbreviations, see figure 1. Sed = sedimentary minerals, Met = metamorphic minerals, 1 = mélange zone, 2 = D_4 shear zones in schists and phyllites within the Berinag Group quartzites.

M. Wyss

Plate 1 Sections for the Spiti valley–eastern Lahul-Parvati valley area.